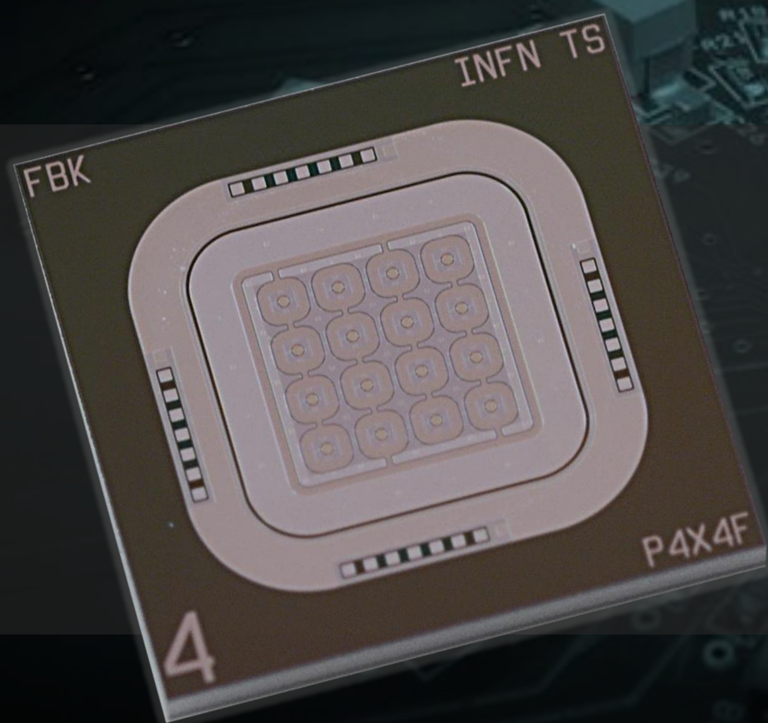

X-ray diagnostics and technologies for High Energy Astrophysics

Yuri Evangelista
INAF/IAPS, INFN – Roma 2

ESA "COSMIC VISION"

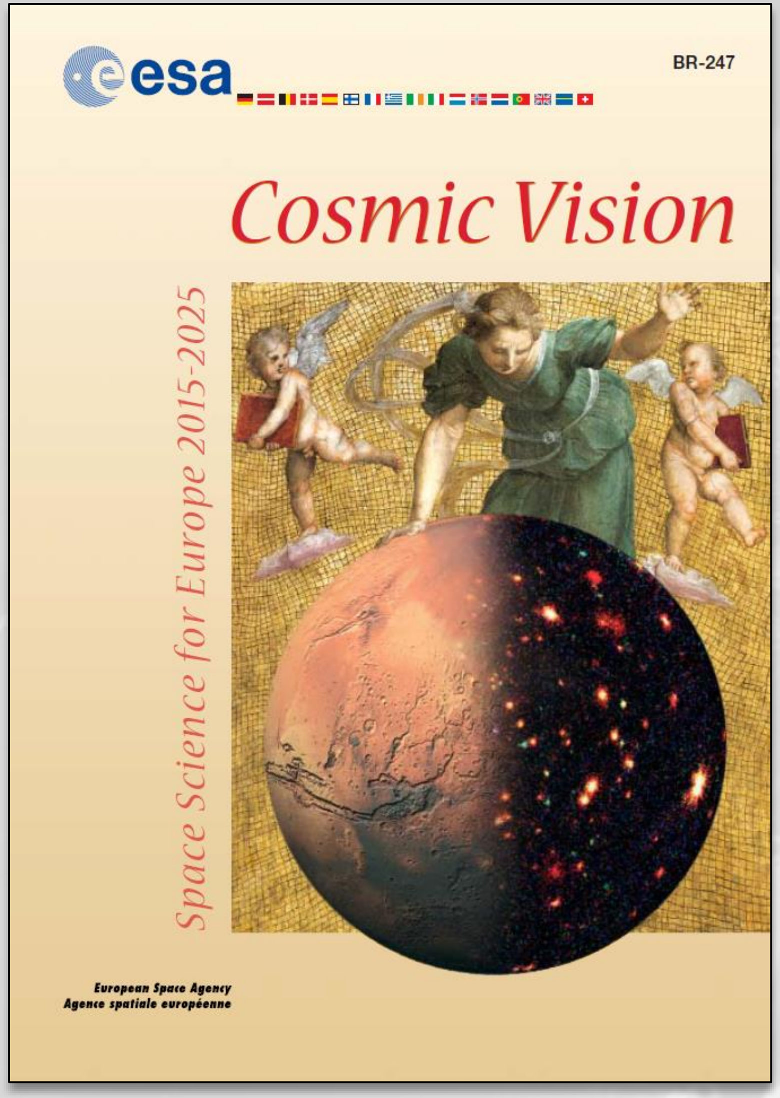

In 2005, ESA's Space Science Advisory Committee (SSAC) prepared the Cosmic Vision plan.

[...] The team preparing Cosmic Vision 2015-2025 has subdivided the four main questions by selecting areas where major progress can be expected in the next two decades.

[...] Cosmic Vision 2015-2025 addresses four main questions that are high on the agenda of research across Europe (and, indeed, worldwide) concerning the Universe and our place in it.

ESA "COSMIC VISION"

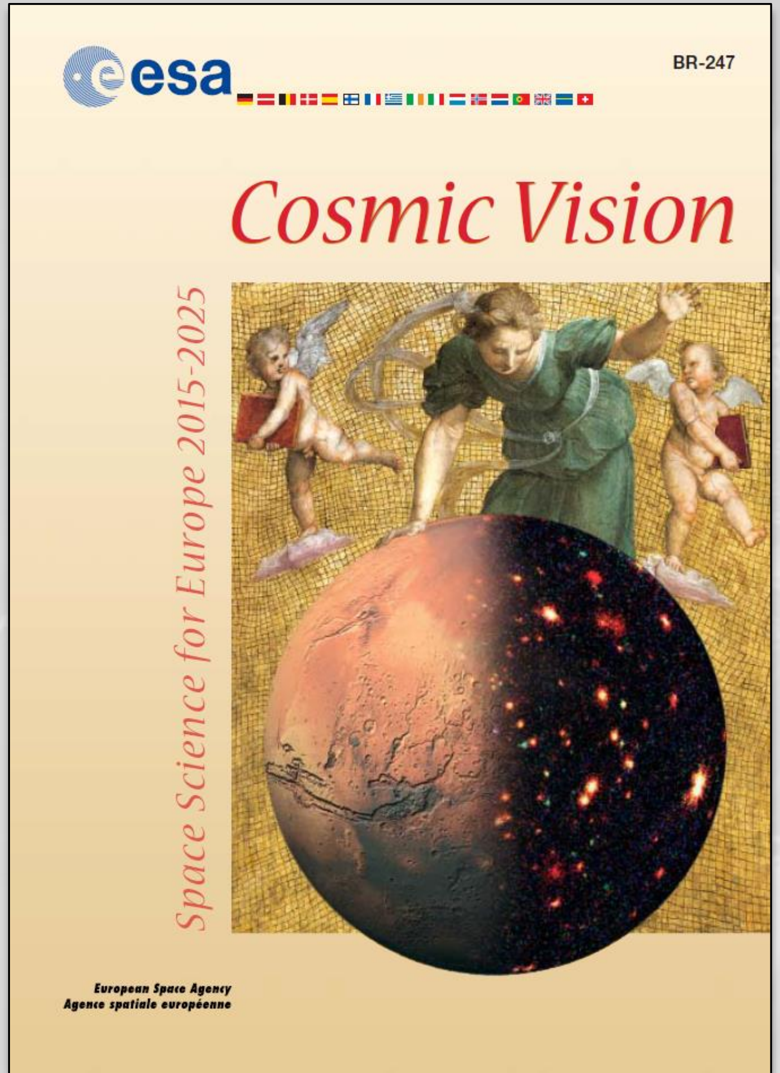

Toolkit for Theme 3

	Tools
3. What are the fundamental physical laws of the Universe?	
3.1 Explore the limits of contemporary physics	
Probe the limits of general relativity, symmetry violations, fundamental constants, short-range forces, quantum physics of Bose-Einstein condensates, and ultra-high-energy cosmic rays, to look for clues to unified theories	
Use the stable and gravity-free environment of space to implement high-precision experiments to search for tiny deviations from the standard model of fundamental interactions	*Fundamental physics explorer programme*
Test the validity of Newtonian gravity using a trans-Saturn drag-free mission	*Deep space gravity probe*
Observe from orbit the patterns of light emitted from the Earth's atmosphere by the showers of particles produced by the impacts of sub-atomic particles of ultra-high-energy	*Space detector for ultra-high-energy cosmic rays*
3.2 The gravitational wave Universe	
Make a key step towards detecting and studying the gravitational radiation background generated at the Big Bang. Probe the Universe at high redshift and explore the dark Universe	
Primordial gravitational waves, unaffected by ionised matter, are ideal probes of the laws of physics at the fantastic energies and temperatures of the Big Bang. They open an ideal window to probe the very early Universe and dark energy at very early times	*Gravitational wave cosmic surveyor*
3.3 Matter under extreme conditions	
Probe general relativity in the environment of black holes and other compact objects, and investigate the state of matter inside neutron stars	
The study of the spectrum and time variability of radiation from matter near black holes shows the imprint of the curvature of space-time as predicted by general relativity. This has strong implications for astrophysics and cosmology in general	*Large-aperture X-ray observatory*

THEME 3
THE X-RAY "VIEW"

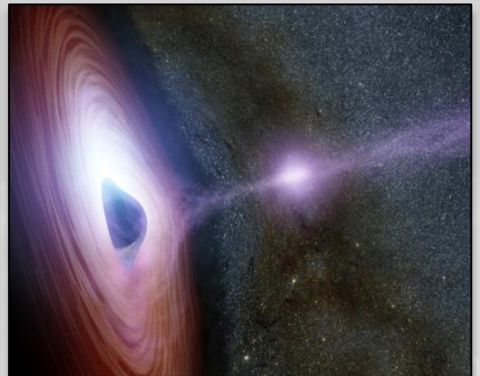

Matter in the strong-field regime
behaviour of matter close to galactic and extragalactic black holes (XRBs, AGNs), test of GR predictions and accretion physics models

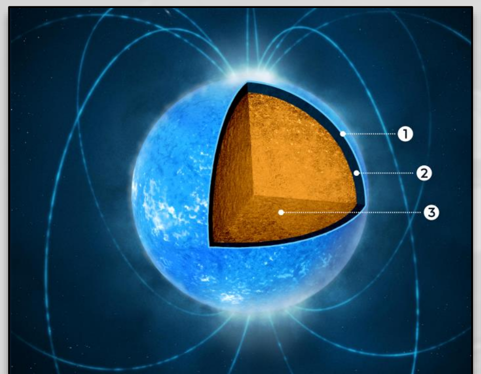

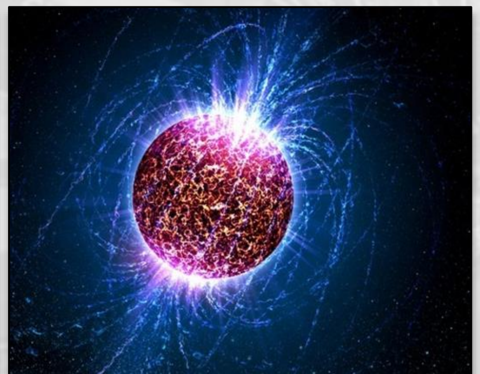

Dense matter
EOS at high density, low temperature in NSs

Physics in extremely strong magnetic fields
accretion processes, birefringence, QED effects in highly magnetized star (magnetars)

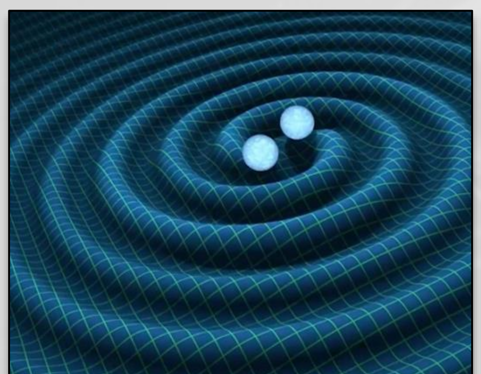

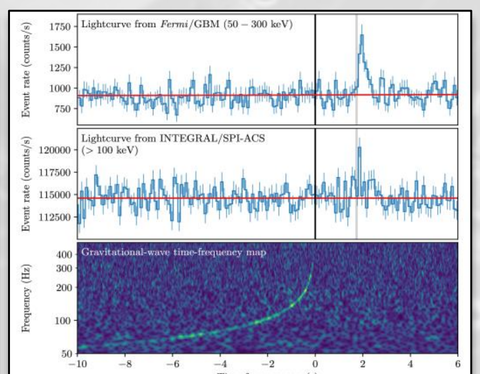

GW and multi-messenger astronomy
monitor and detect NS-NS and NS-BH mergers providing real-time, precise positioning

3.3 Matter under extreme conditions

Probe general relativity in the environment of black holes and other compact objects, and investigate the state of matter inside neutron stars

The study of the spectrum and time variability of radiation from matter near black holes shows the imprint of the curvature of space-time as predicted by general relativity. This has strong implications for astrophysics and cosmology in general

Large-aperture X-ray observatory

Table 5.4.3.1: The technologies required for the development of an X-ray facility focused on the X-ray temporal properties.

Technology	*Comment*
High time-resolution sensors	Rates > 1 MHz and resolution ~1 μs
Precision clocks	Absolute local time to 100 ns
Higher energy mirror systems	Layered synthetic microstructures
High-energy X-ray semiconductors	Imaging arrays
Spectropolarimeters	High sensitivity

STRONG FIELD GRAVITY

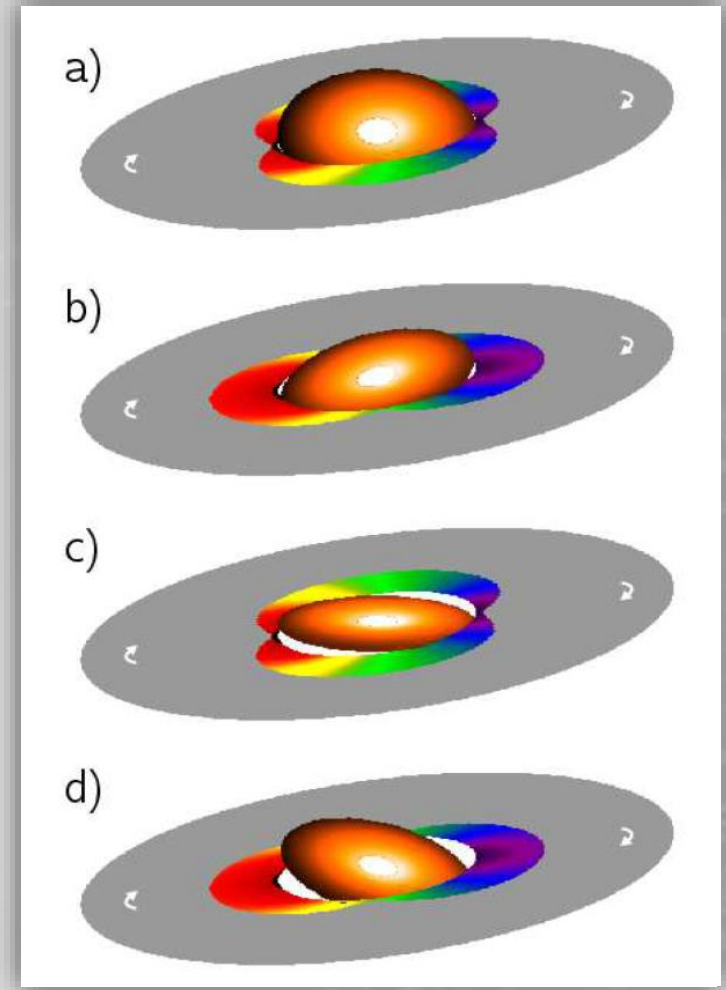

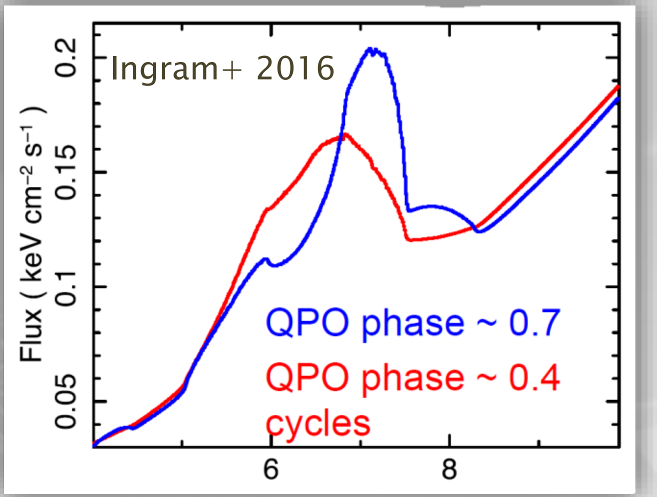

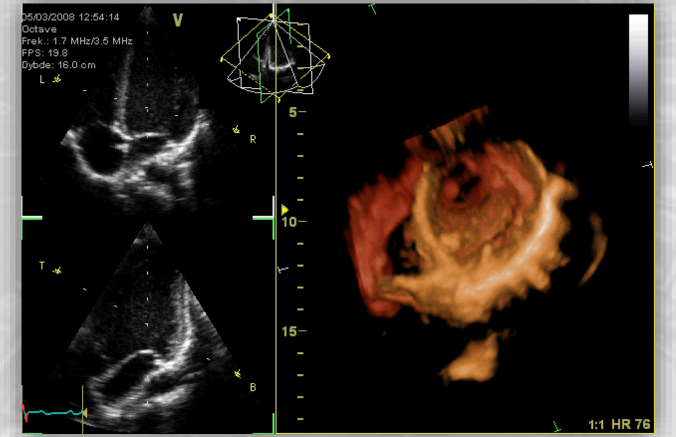

Precession due to Lense-Thirring effect (Stella & Vietri 1998)

General relativistic frame-dragging of orbiting plasma, caused by misalignment of BH spin and the angular momentum of the accreting material in the disk → rocking Iron fluorescence line

DISK TOMOGRAPHY WITH LFQPO

Low frequency ($10^{-1} \div 10^{1}$ Hz) Quasi Periodic Oscillation (QPO)
Phase-resolved spectroscopy (here 2 phases shown)

courtesy of Adam Ingram

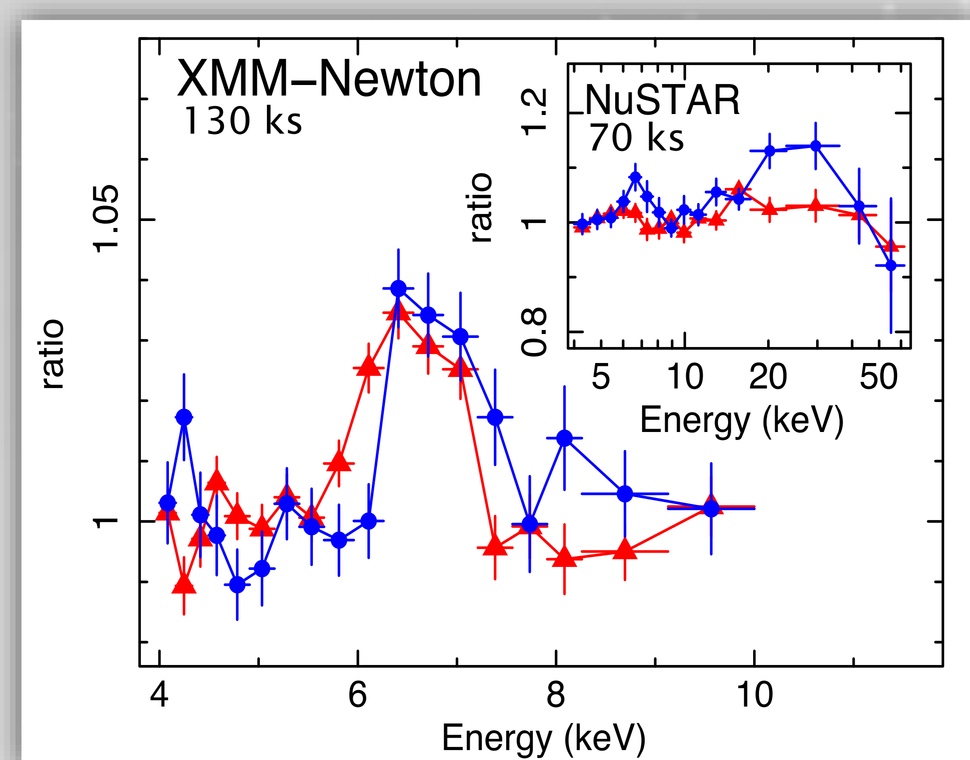

H 1743–322

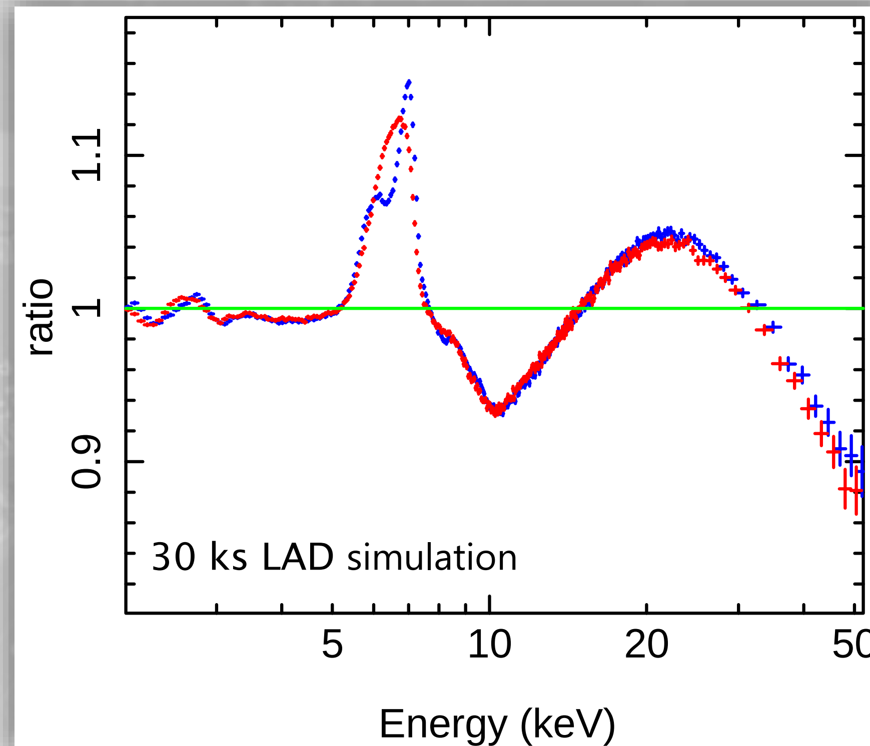

GX 339–4

Follows the motion of matter towards the inner disk radius (r/rg measured at <2% CL) providing information on **disk inclination** (few deg.), **disk inner truncation radius** (few %), disk shape and emission process, **BH mass** (<30%)

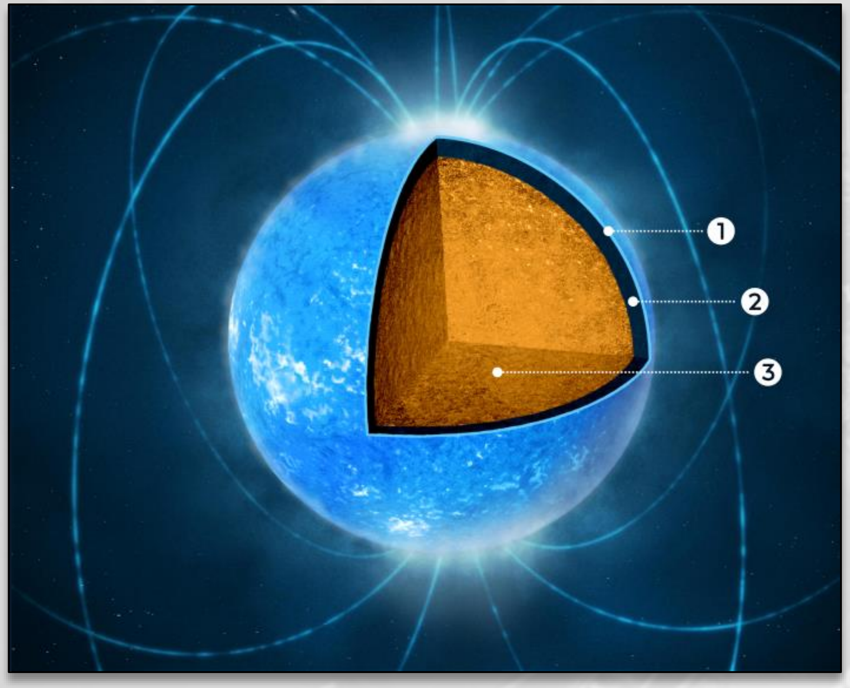

DENSE MATTER

Stellar structure equations

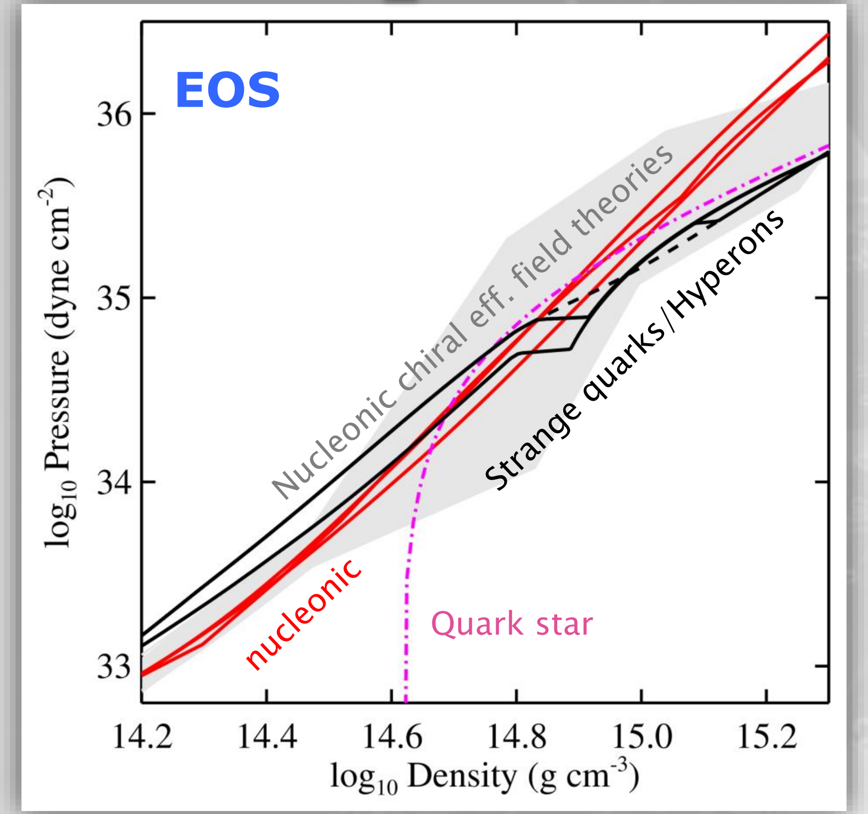

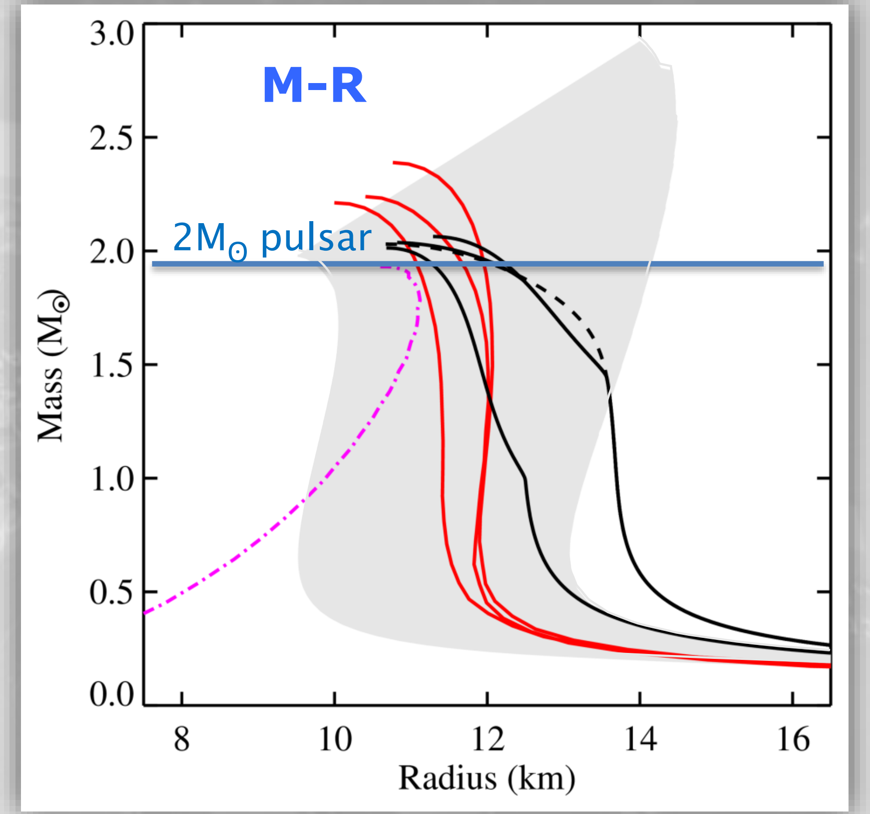

Must measure **both M and R** to **high precision**
(low statistical and systematic errors)

Stellar structure equations

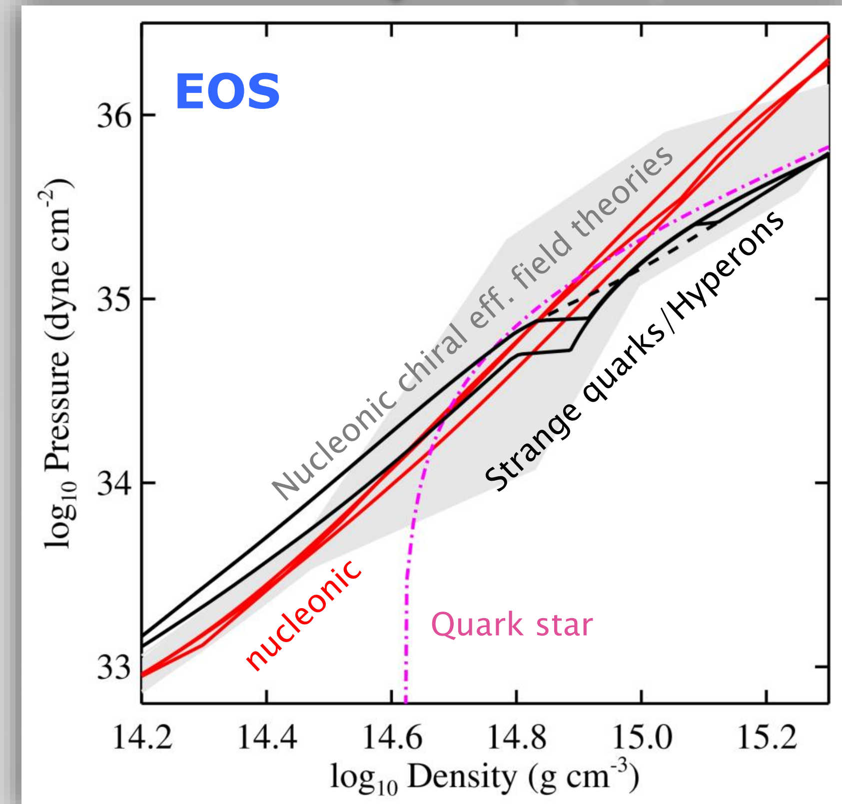

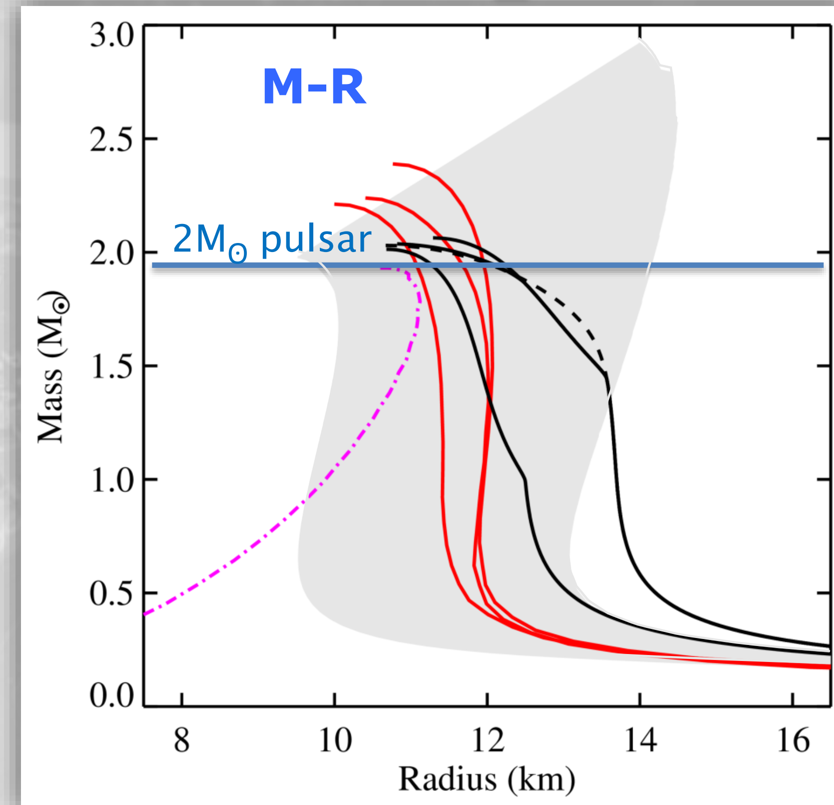

Must measure **both M and R** to **high precision**
(low statistical and systematic errors)

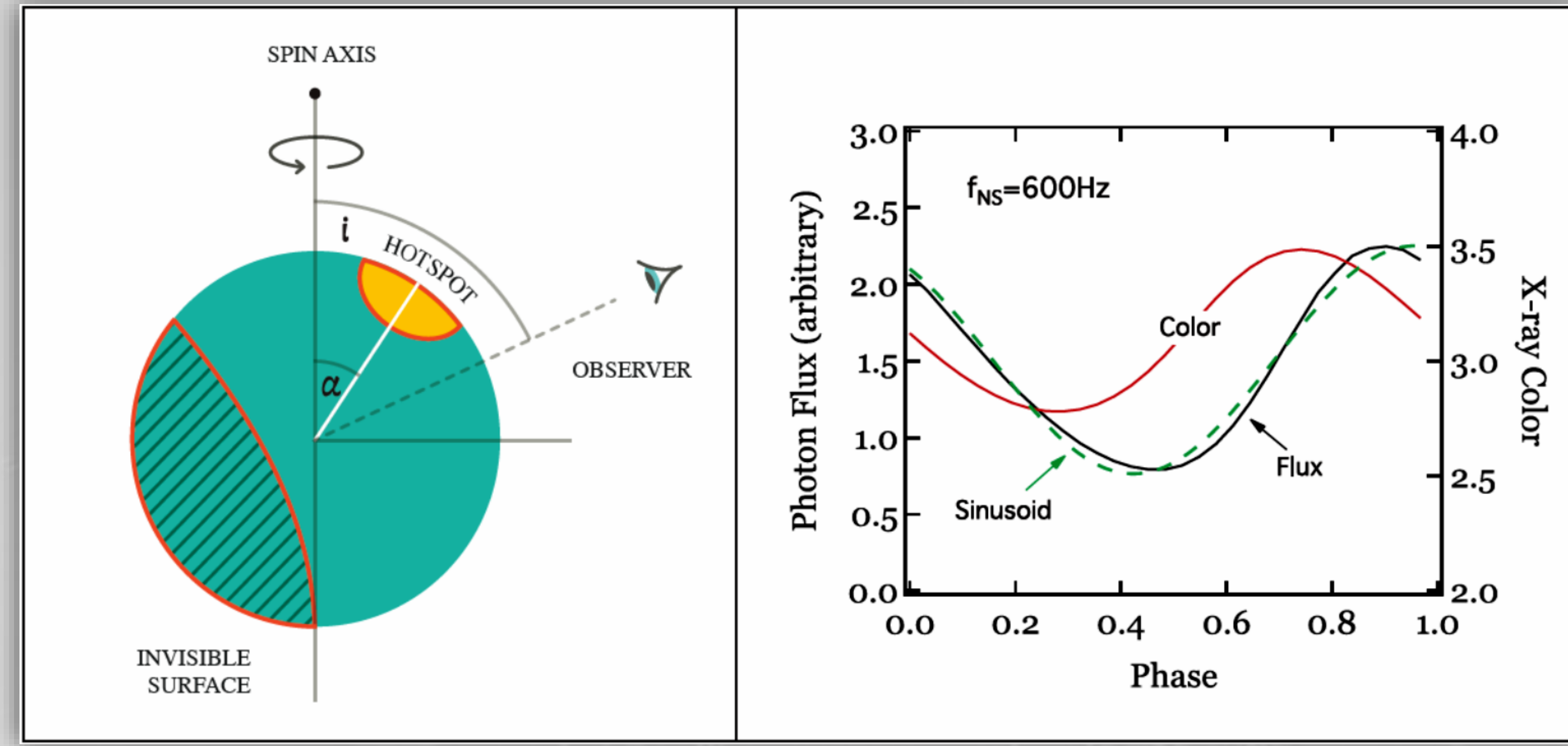

Watts+2016

- Gravitational lensing (M) deforms pulse profile (spin)
- GR light-bending (M/R) affects pulse amplitude
- Doppler boosting (R,spin) change color as a function of phase

Stellar structure equations

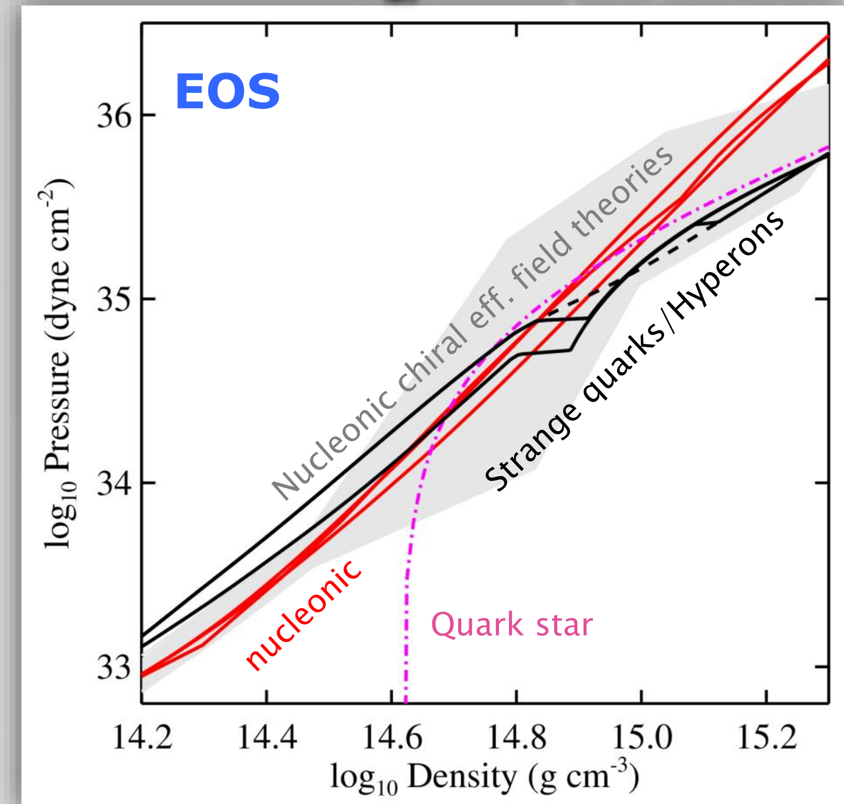

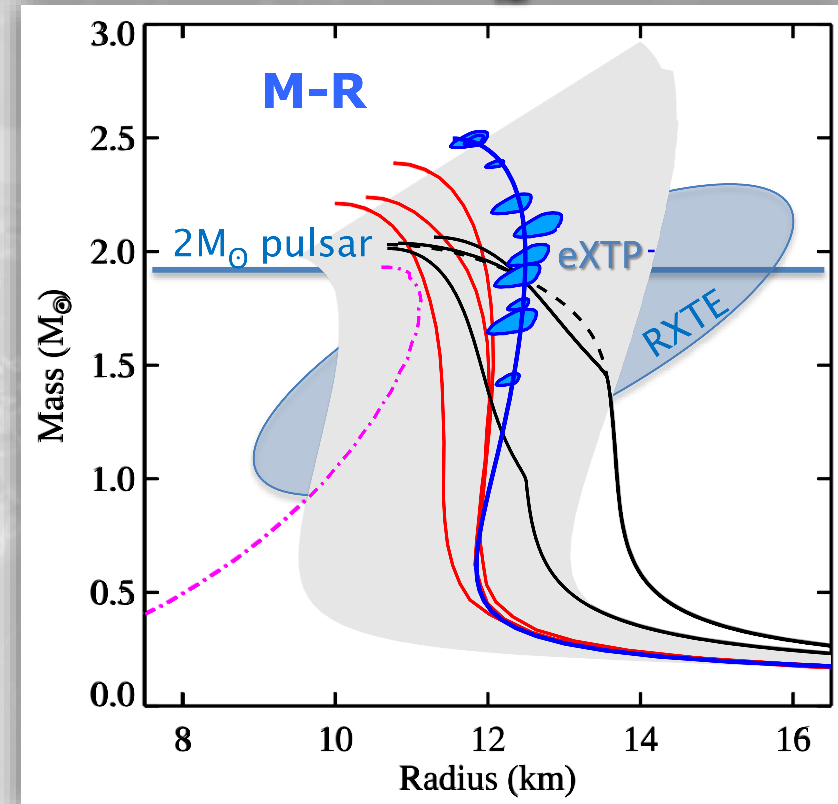

Must measure **both M and R** to **high precision**
(low statistical and systematic errors)
for a **range of M.**

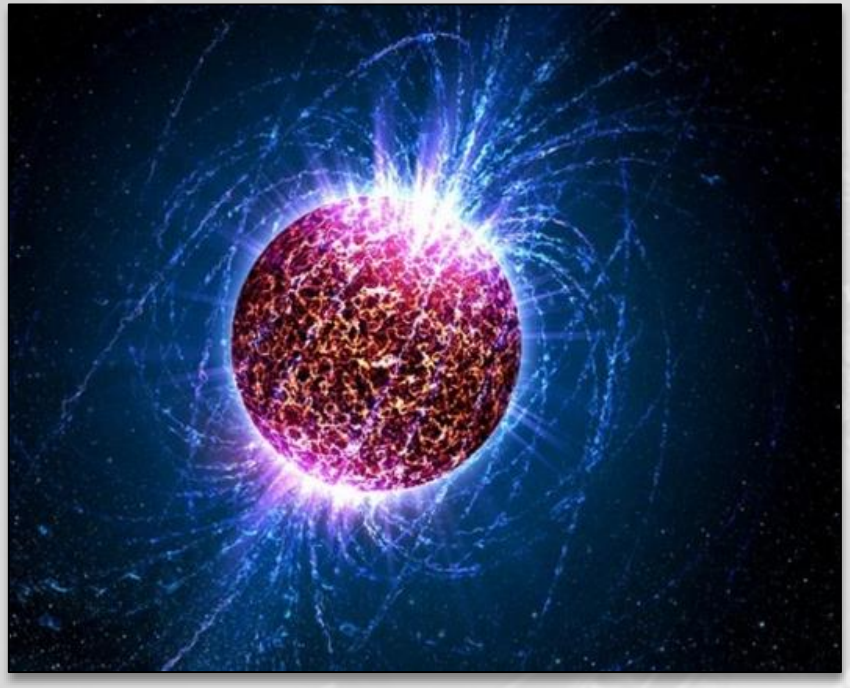

STRONG MAGNETISM

VACUUM BIREFRINGENCE IN MAGNETARS

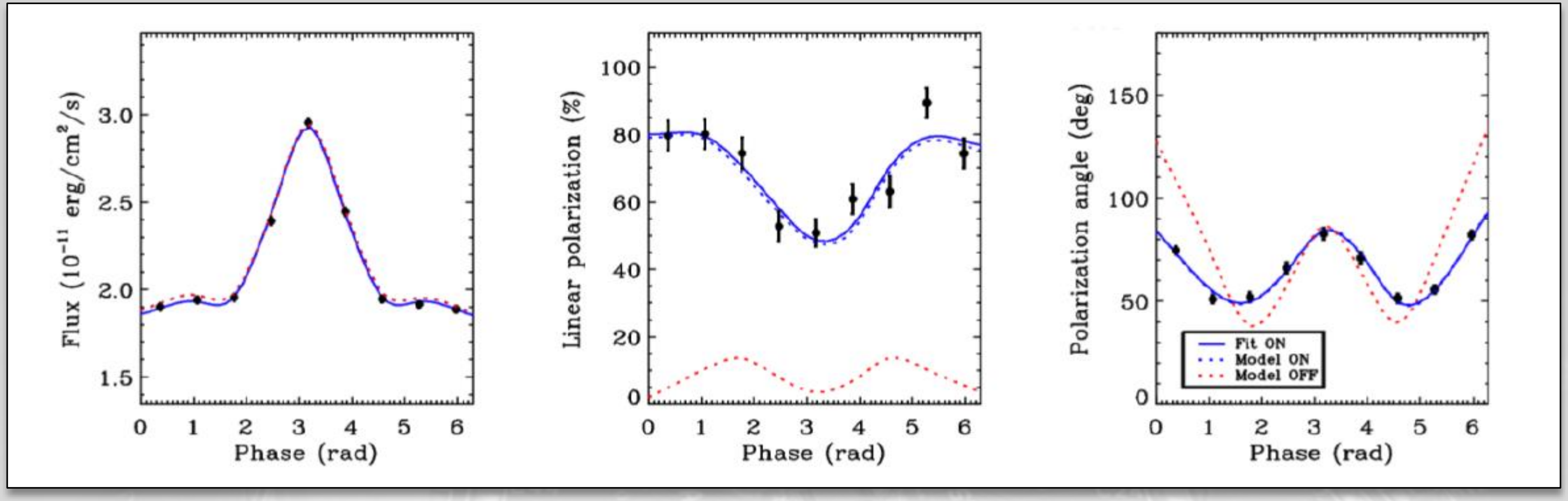

Magnetar is a neutron star with magnetic field up to 10^{15} Gauss

- Non-linear QED predicts birefringence in magnetized vacuum
- Impacts polarization and position angle as functions of pulse phase
- 250 ks simulated IXPE observation to exclude QED-off

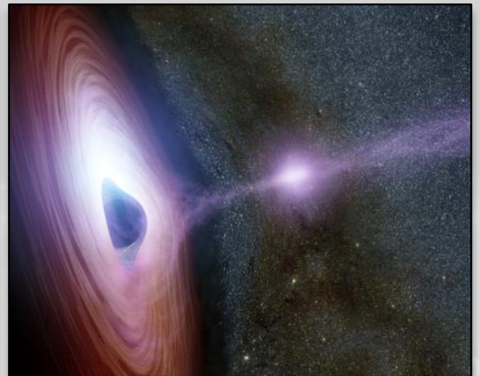

Strong field gravity
- high sensitivity
- good spectral resolution
- good timing resolution
- soft X-ray energy band
- negligible dead-time and pile-up

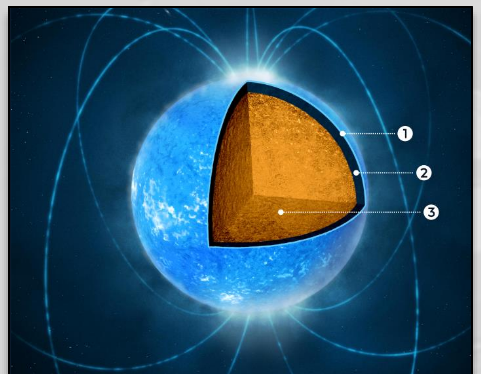

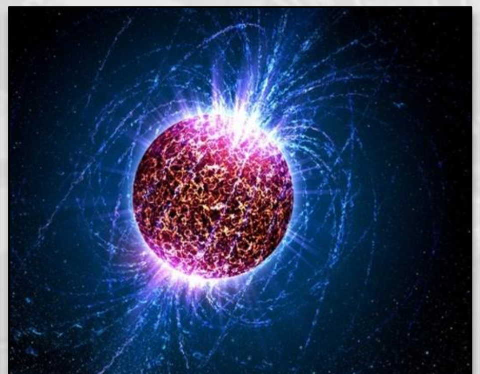

Dense matter
- high sensitivity
- average spectral resolution
- good time accuracy
- soft X-ray energy band
- negligible dead-time and pile-up

Strong magnetic fields
- high sensitivity
- soft X-ray polarimetry

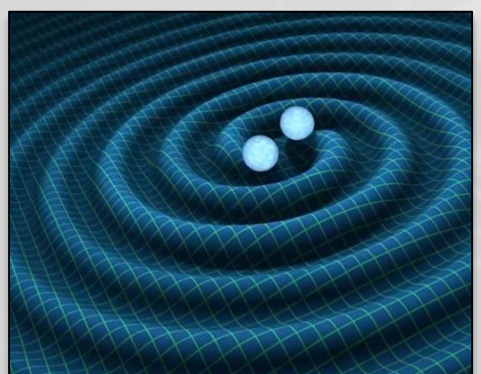

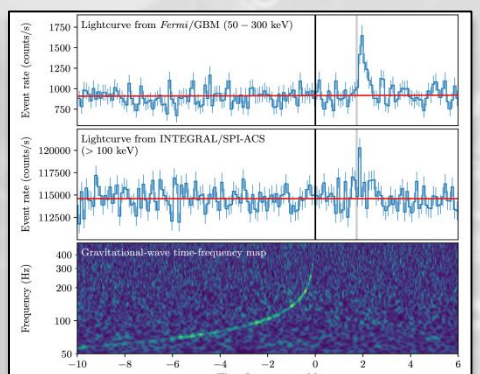

GW and multi-messenger astronomy
- large field-of-view
- good sensitivity
- good angular resolution (PSLA)
- soft/hard X-ray energy band


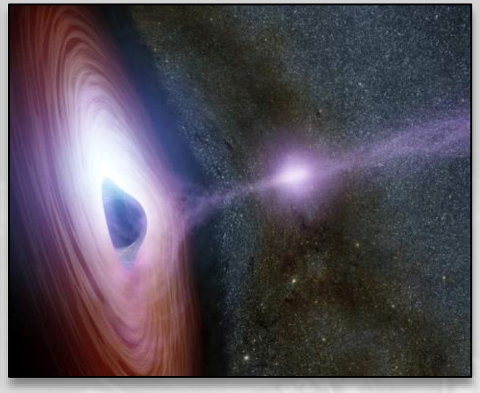

Strong field gravity

- high sensitivity
- good spectral resolution
- good timing resolution
- soft X-ray energy band
- negligible dead-time and pile-up

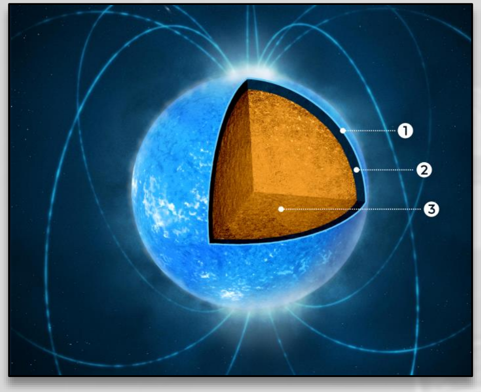

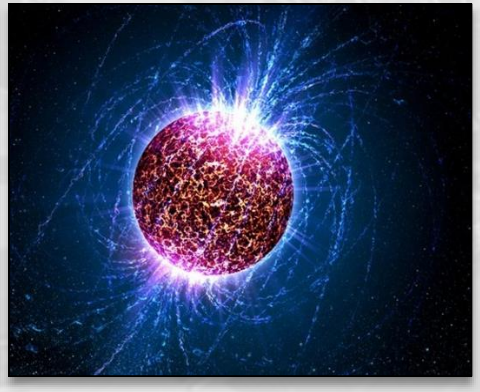

Dense matter

- high sensitivity
- average spectral resolution
- good time accuracy
- soft X-ray energy band
- negligible dead-time and pile-up

Strong magnetic fields

- high sensitivity
- soft X-ray polarimetry

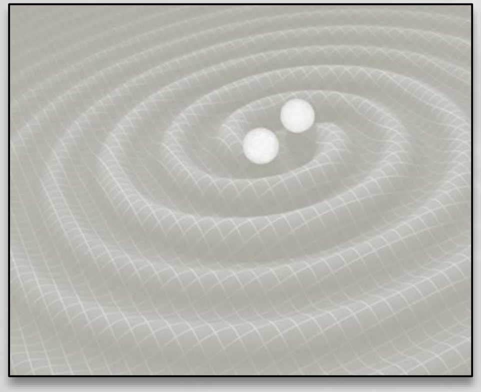
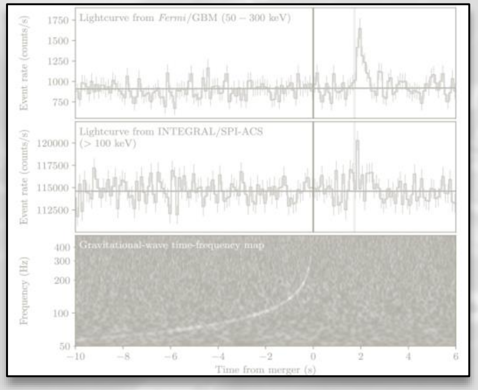

GW and multi-messenger astronomy

- large field-of-view
- good sensitivity
- good angular resolution (PSLA)
- soft/hard X-ray energy band

IXPE – NASA

eXTP - CAS

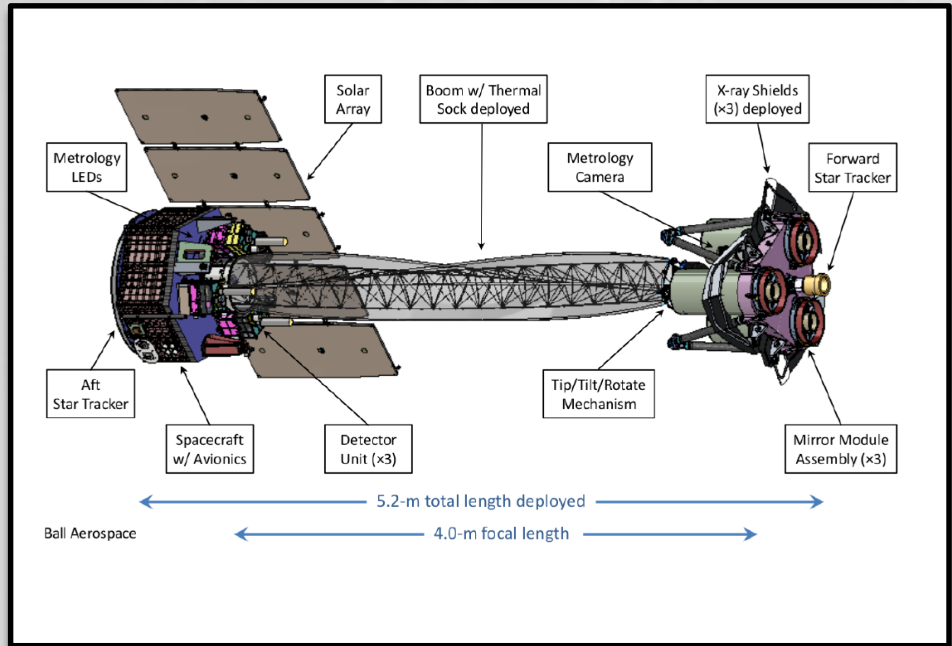

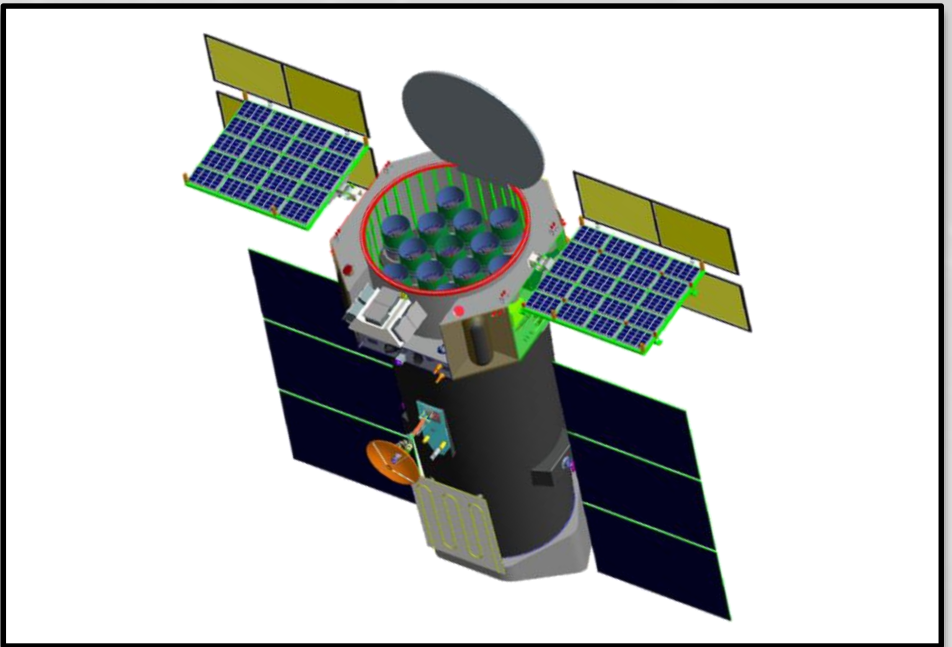

Approved – Launch end 2021

Phase B in early 2019 – Launch ≥ 2025

X-RAY POLARIMETER


Radio (VLA)

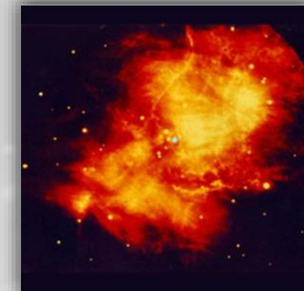
Infrared (Keck)


Optical (Palomar)

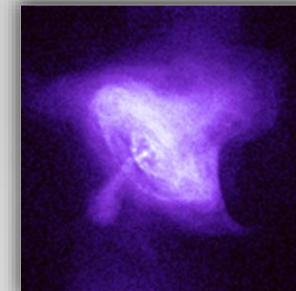
X-rays (Chandra)

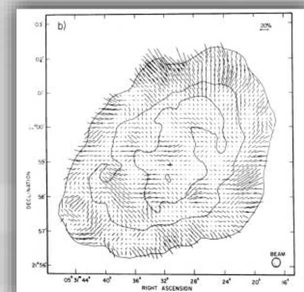
Radio polarisation

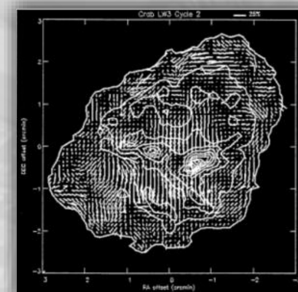
IR polarisation

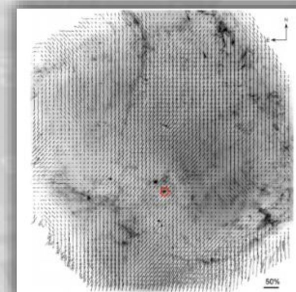
Optical polarisation

?

P=19% integrated over the entire nebula (Weisskopf et al. 1978)

X-ray polarisation

Polarization is a common tool at many wavelengths

(linear) polarization naturally arises in:

- sources which emits X-rays emission from accretion disks, with the “preferred” direction set by the disk
- non-thermal emission (e.g. synchrotron, the “preferred” direction is set by the magnetic field)
- radiative transfer in a strong gravitational/magnetic field (e.g. magnetized plasma are birefringent)

Basically all classes of X-ray sources should emit partially pol. radiation at a few % level

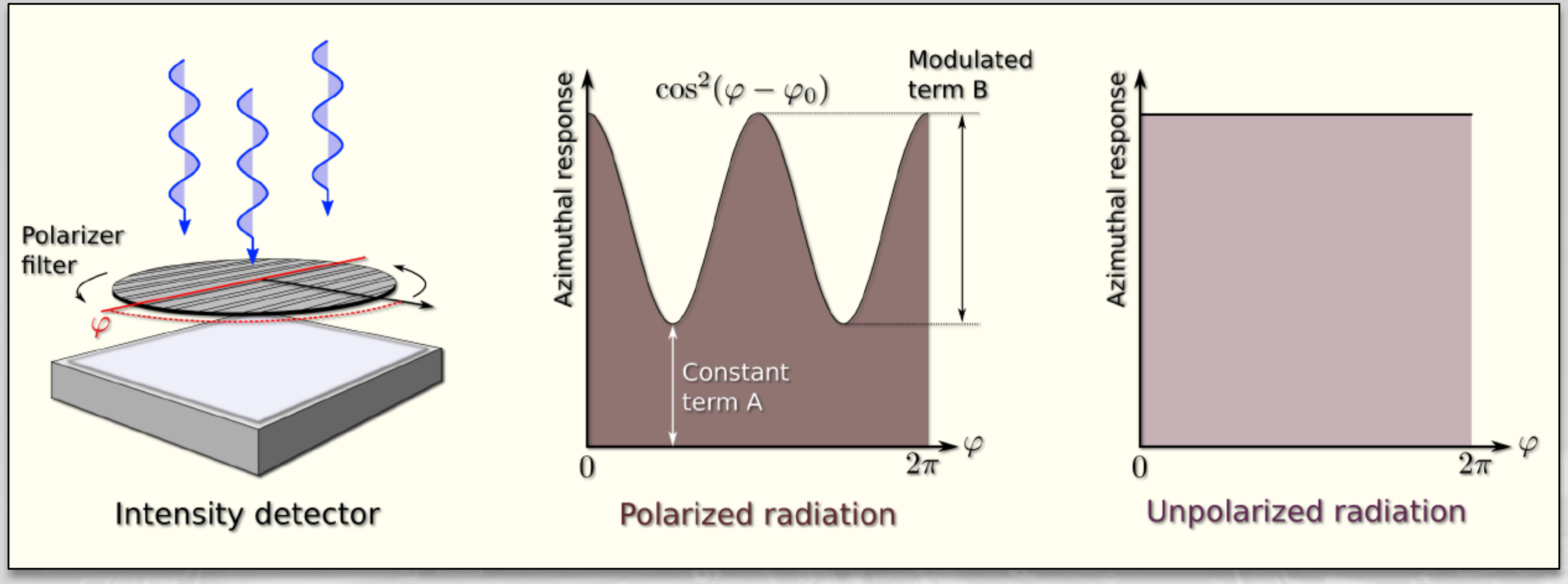

Degree of polarization P

- proportional to the modulation amplitude, B/(B+2A)
- the constant of proportionality is the **modulation factor μ** (defined as the amplitude of the measured modulation for 100% polarized photons)

Angle of polarization Φ_0

- related to the phase of the measured modulation curve φ_0
- $\Phi_0 = \varphi_0$ for a photoelectric polarimeter ($\Phi_0 = \varphi_0 + \pi/2$ for Compton polarimeters)

Costa et al. 2001
Bellazzini et al. 2006, 2007

Distribution of the direction of emission of a K-shell photoelectron 100% modulated for linearly polarized radiation

latitudinal dependency

azimuthal dependency

$$\frac{d\sigma_{ph}^{K}}{d\Omega} \propto Z^5 \left(\frac{m_e c^2}{E}\right)^{\frac{7}{2}} \frac{4\sqrt{2}\sin^2\theta\cos^2\phi}{(1+\beta\cos\theta)^4}$$

"relativistic correction" to the lat. dependency

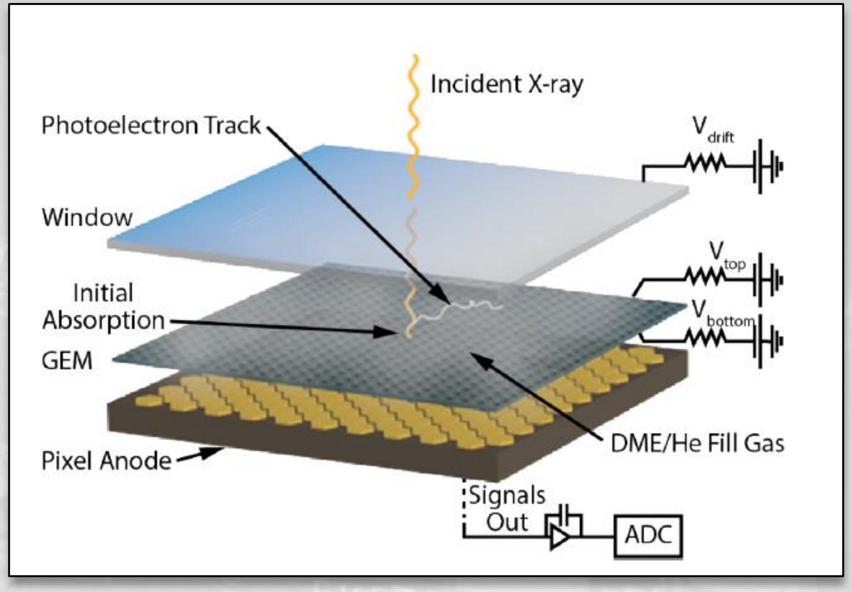

Need to reconstruct the direction of emission of the photoelectron, i.e., a granularity significantly smaller than the typical range of the photoelectron is required

Detector concept:

- X-ray absorption in a gas cell
- Amplification via a Gas Electron Multiplier (GEM)
- Finely pixelized ASIC as readout anode
- Sensitive down to low energy (2÷8 keV)
- Fully two-dimensional (imaging)

THE PHOTOELECTRIC POLARIMETER

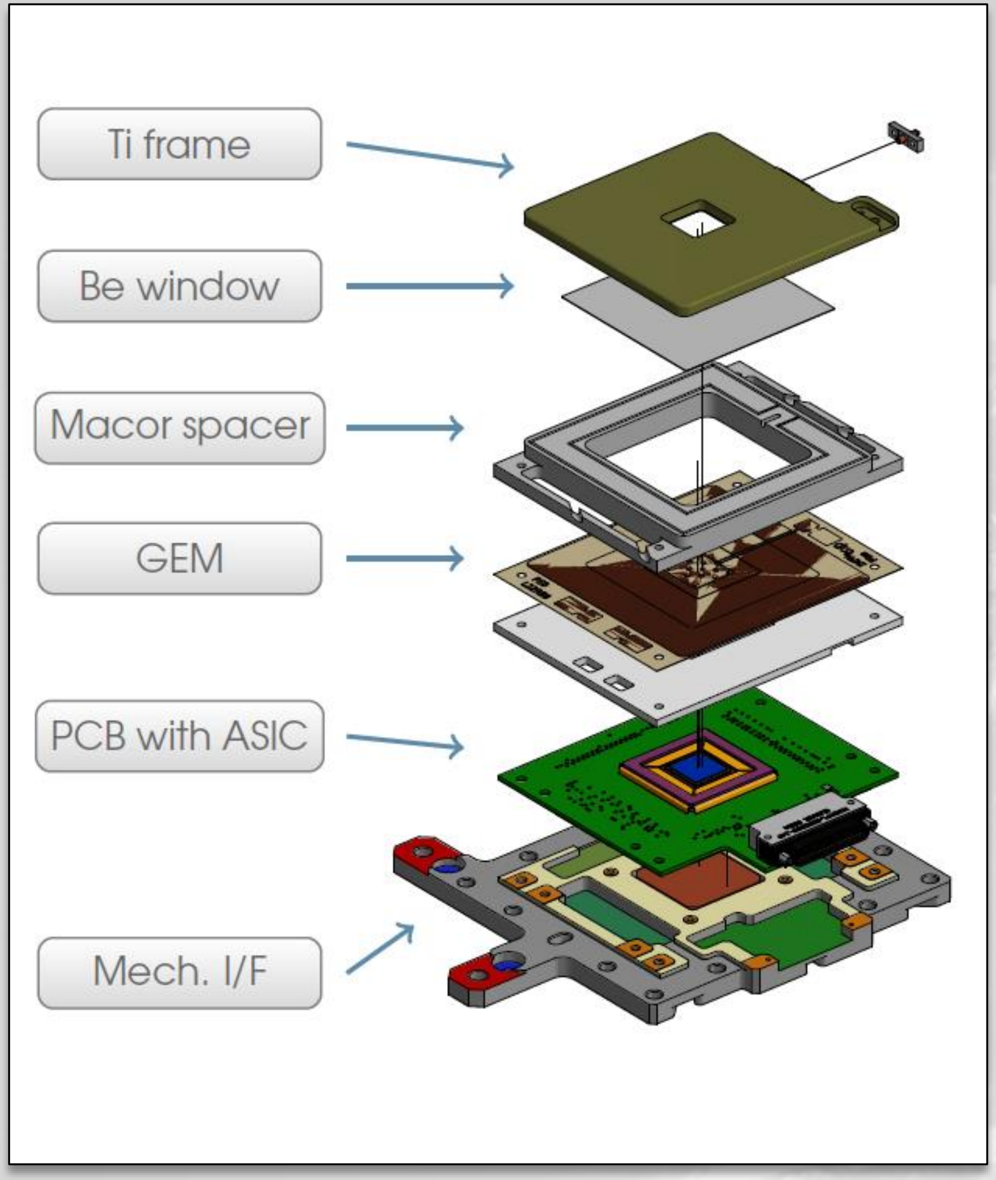

IXPE Polarimeter

- Sealed detector
- No gas system needed
- Gas cell thickness 1 cm
- He - DME (small lateral diffusion)
- Optimized in the 2-8 keV range
- Ti frame acts as “drift” electrode
- X-ray window in Be, 50 μm thick
- GEM holes 50 μm pitch, 50 μm thick
- Packaged ASIC on a custom PCB
- Ti frame for mechanical and thermal I/F

READ-OUT ASIC

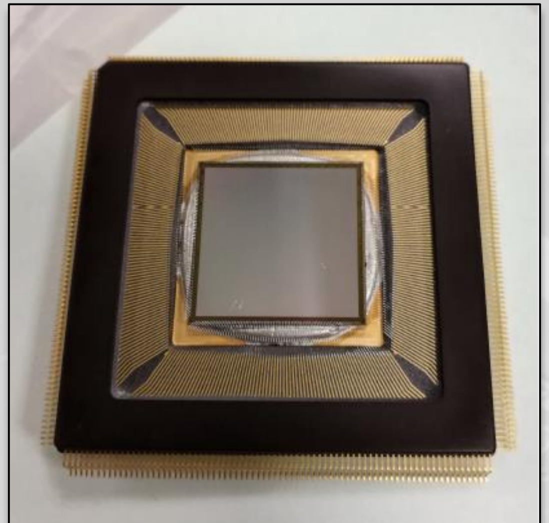

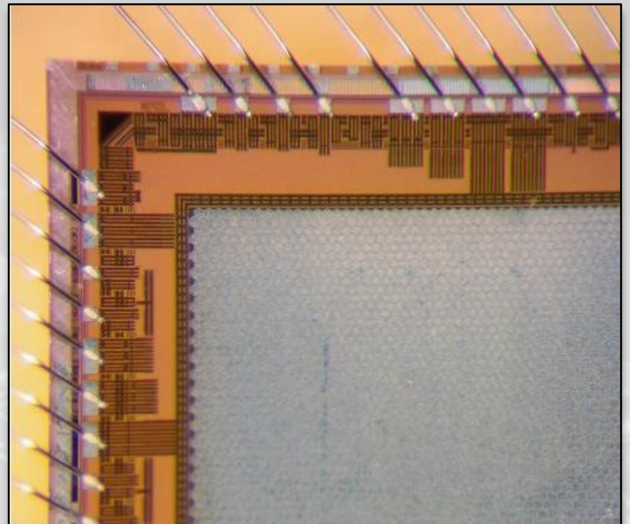

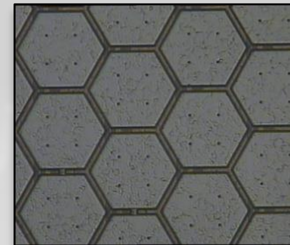

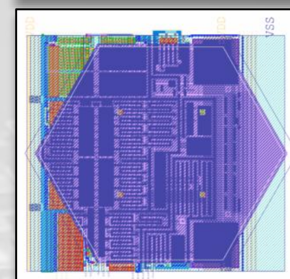

Pixels organization	300×352 pixels in hexagonal pattern
Pixel pitch	50 μm
Active area	15×15 mm^2
Shaping time	3-10 μs
Pixel Noise	$\sim$ 50 electrons ENC
Trigger	internal, with definition of a region of interest
Output	analog (external ADC required)
Technology	CMOS 0.18 μm

Bellazzini et al. 2006, 2007

GEM

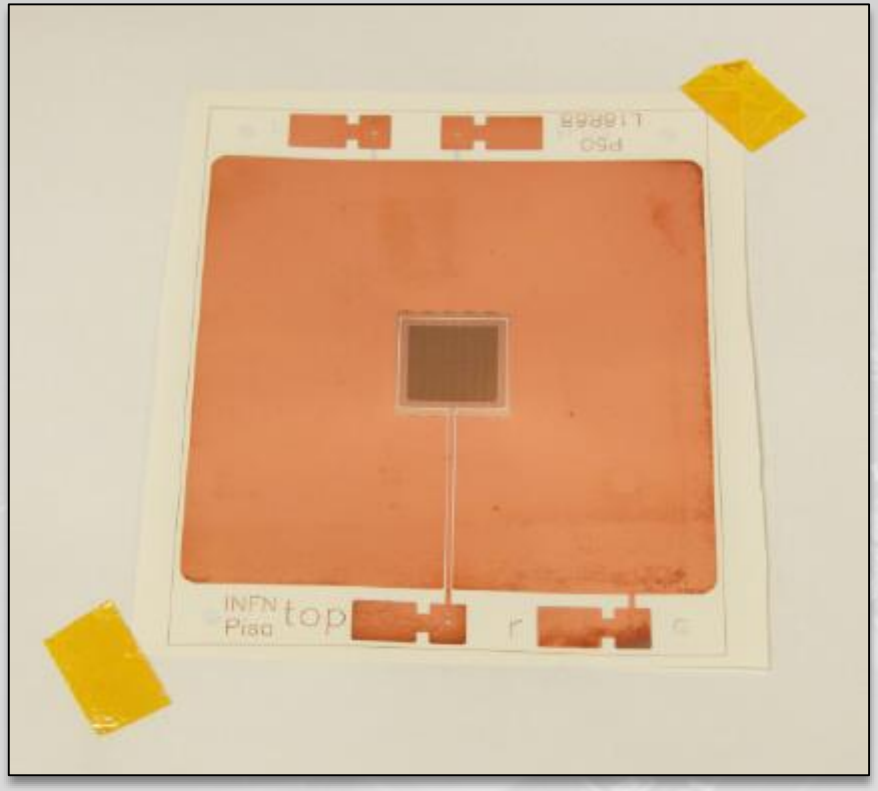

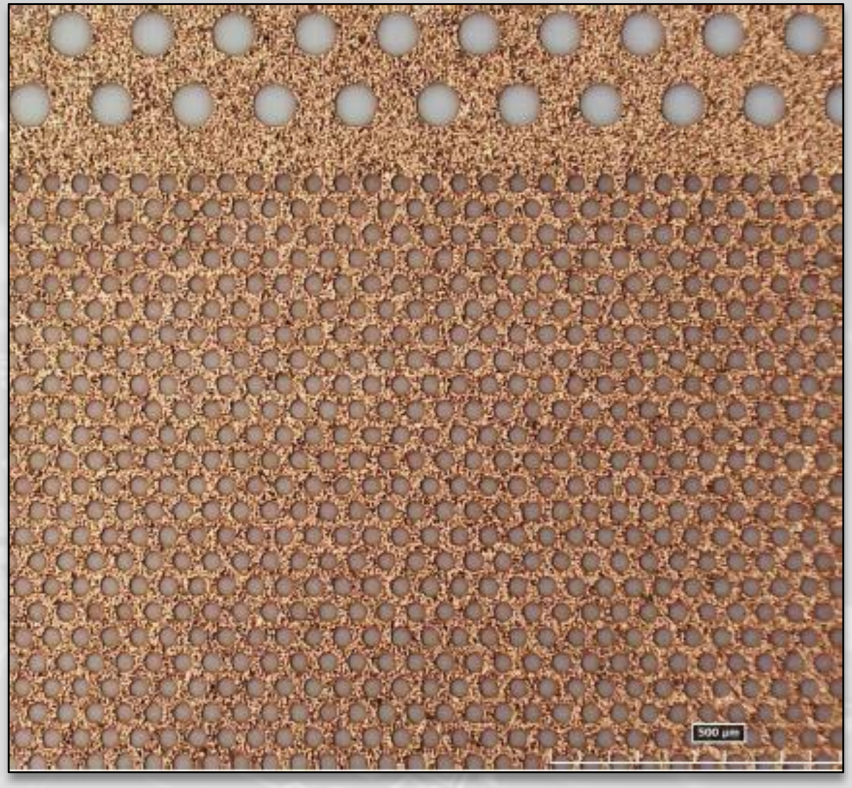

- GEM foil produced by RIKEN and SciEnergy in Japan
- Hexagonal hole pattern, with 50 µm pitch, 50 µm thick

TRACK RECONSTRUCTION ALGORITHM

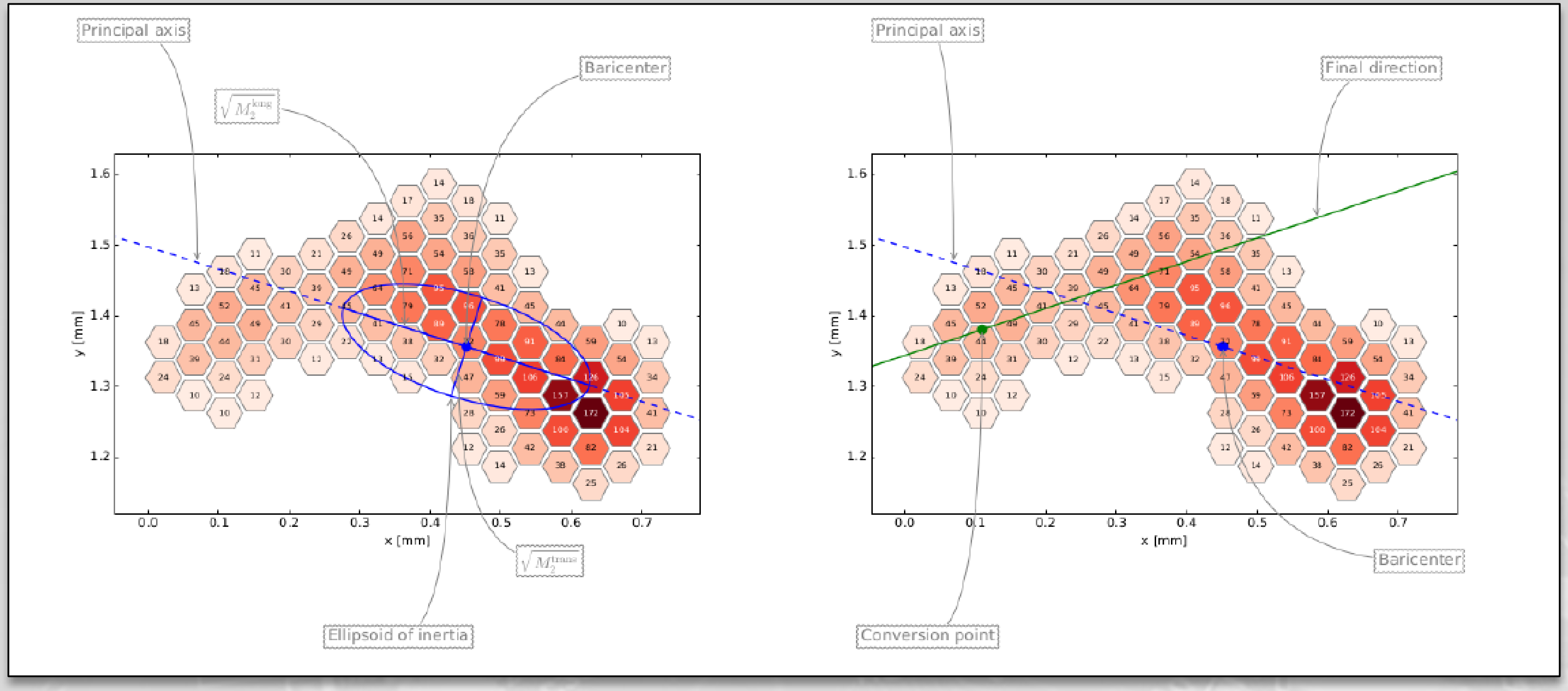

- Event by event reconstruction
- Rich morphological information available
- Iterative moment analysis to reconstruct relevant information
  - Interaction point: **imaging**
  - Photoelectron direction: **polarimetry**
  - Trigger output: **timing**
  - Pixel charge content: **spectroscopy**

PERFORMANCE

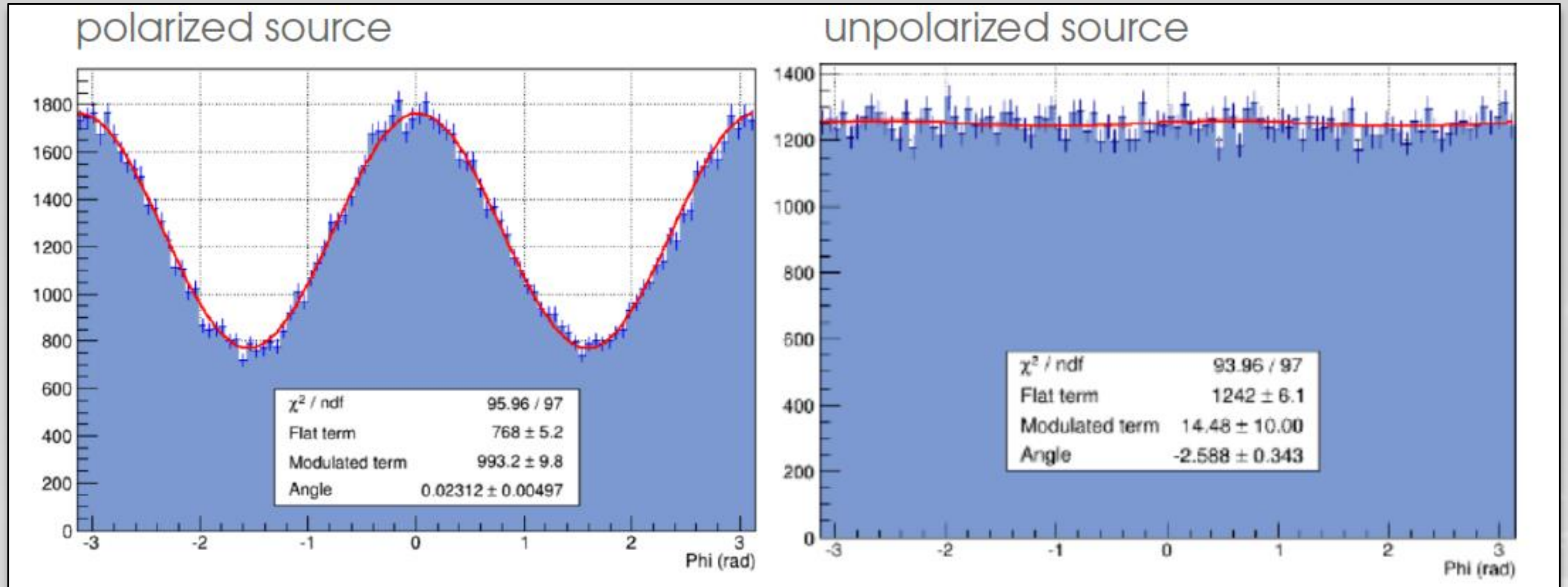

- **Modulation factor**: 0.2 (0.7) at 2 (8) keV
  - Stability over 3 years demonstrated with a sealed detector
- Residual modulation for unpolarized radiation <0.5%
- 90 μm **spatial resolution** at 5.9 keV, measured (track length)
  - Good match for a 25 arcsec-type X-ray optics with 4m focal length
- <20% **energy resolution** (FWHM) at 5.9 keV
  - spectrally-resolved polarimetry (in a few energy bins)
- μs-type **time resolution**
  - More than adequate for the shortest time scales of interest

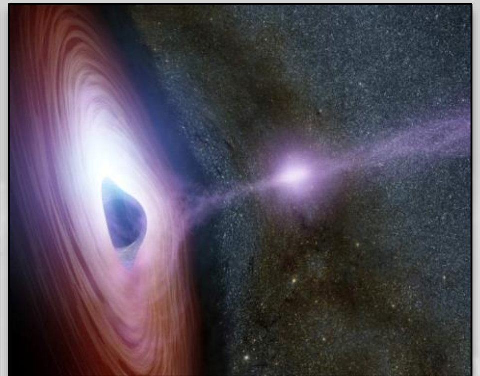

Strong field gravity

- high sensitivity
- good spectral resolution
- good timing resolution
- soft X-ray energy band
- negligible dead-time and pile-up

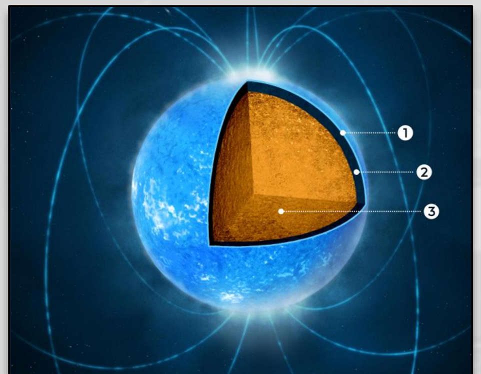

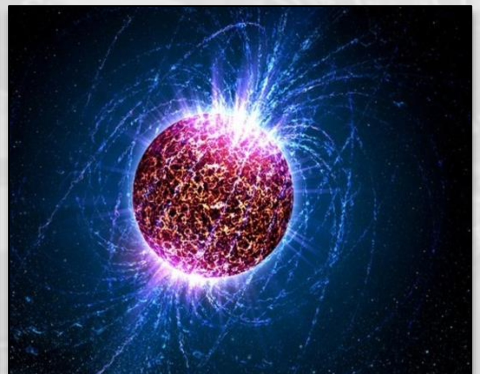

Dense matter

- high sensitivity
- average spectral resolution
- good time accuracy
- soft X-ray energy band
- negligible dead-time and pile-up

Strong magnetic fields

- high sensitivity
- soft X-ray polarimetry

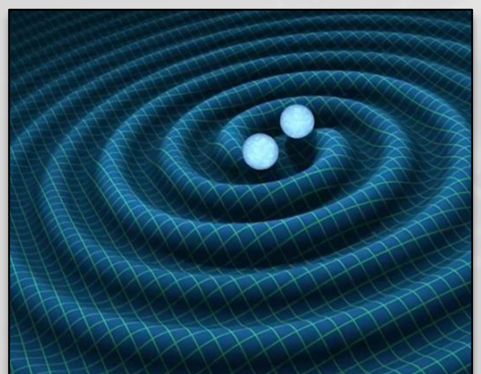

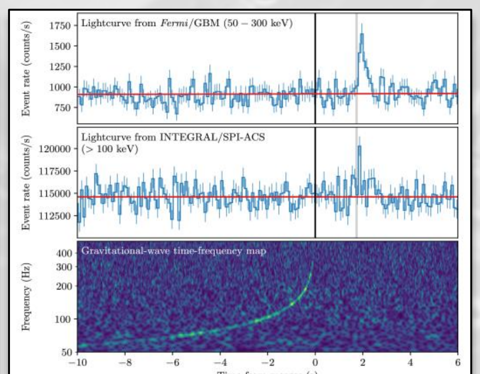

GW and multi-messenger astronomy

- large field-of-view
- good sensitivity
- good angular resolution (PSLA)
- soft/hard X-ray energy band

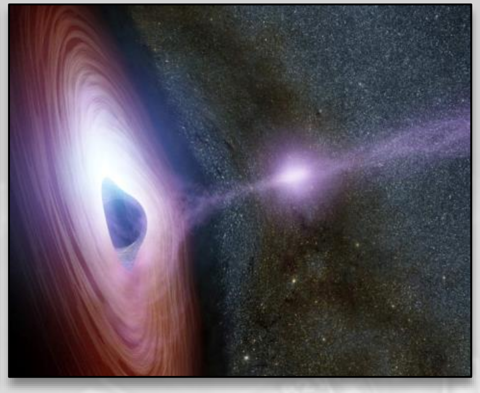

Strong field gravity

- high sensitivity
- good spectral resolution
- good timing resolution
- soft X-ray energy band
- negligible dead-time and pile-up

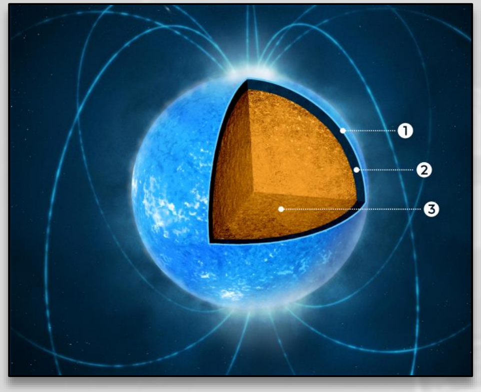

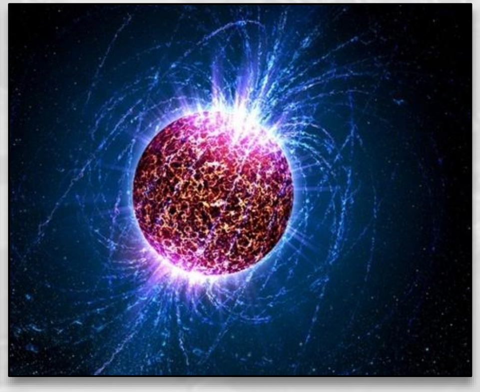

Dense matter

- high sensitivity
- average spectral resolution
- good time accuracy
- soft X-ray energy band
- negligible dead-time and pile-up

Strong magnetic fields

- high sensitivity
- soft X-ray polarimetry

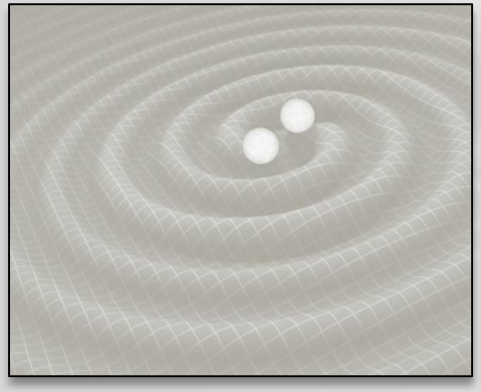

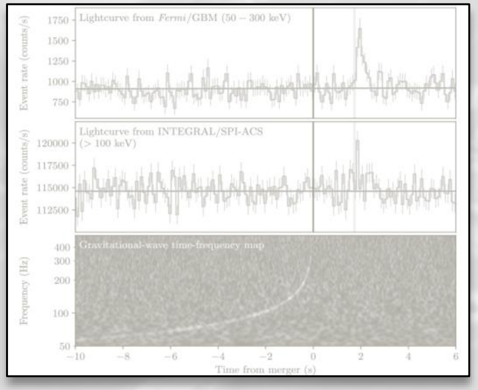

GW and multi-messenger astronomy

- large field-of-view
- good sensitivity
- good angular resolution (PSLA)
- soft/hard X-ray energy band

eXTP - CAS

STROBE-X - NASA

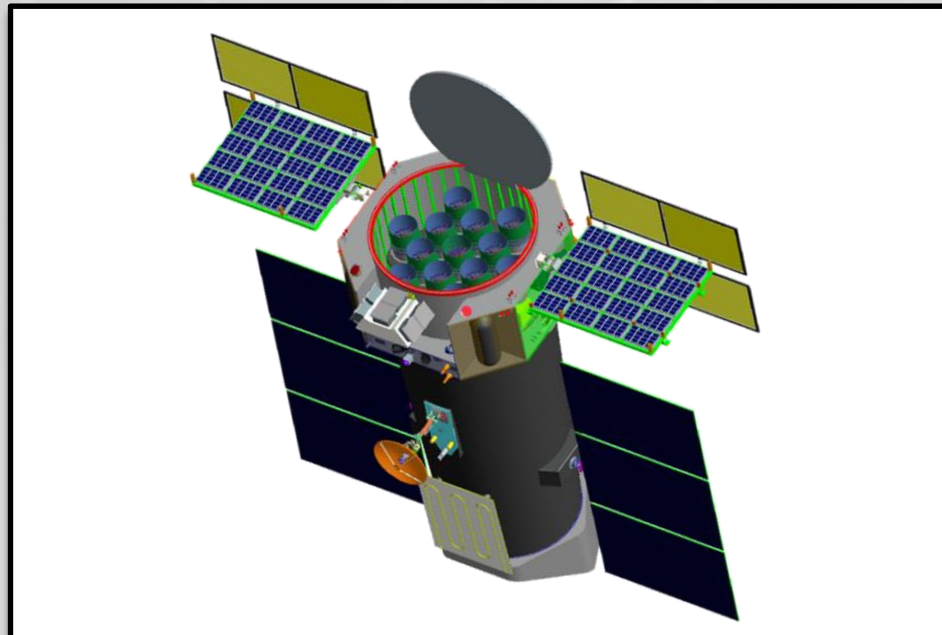

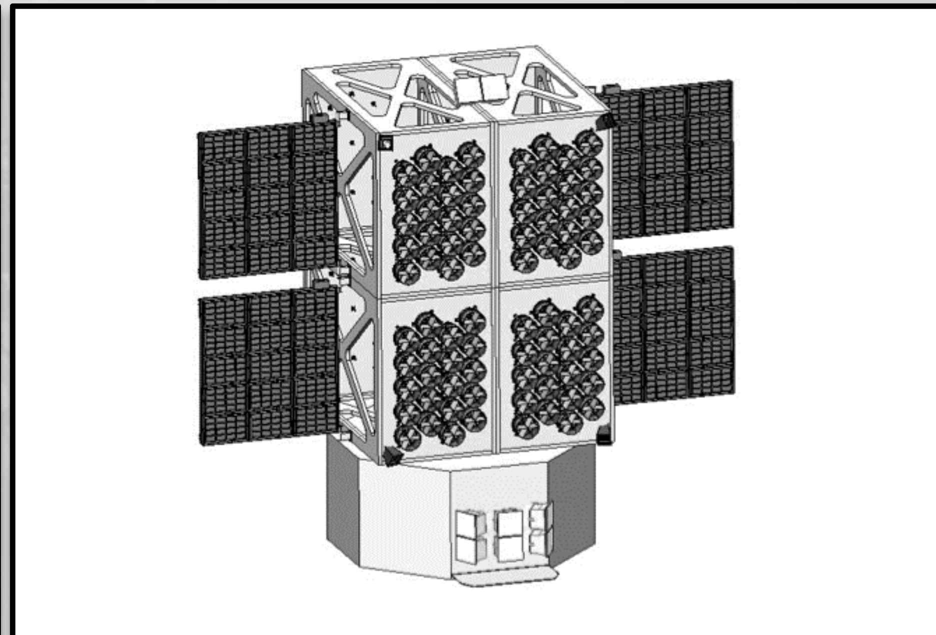

Phase B in 2019 – Launch ≥ 2025

Study for Decadal 2020 survey

$$n_\sigma = \frac{1}{2}\frac{S^2}{B+S} r_S^2 \left(\frac{T}{\Delta\nu}\right)^{1/2}$$

- S: source count rate
- B: background count rate
- r_s: rms amplitude of the variability (S)
- T: integration time
- Δν: variability bandwidth (related to the coherence time)

For signal dominated observations (S>>B), $n_\sigma \sim S$ (i.e. $n_\sigma \sim A$)

Parameter	Requirement
Energy range	2–30 keV
Effective area	~10^4 cm^2
Energy resolution (FWHM, @ 6 keV)	< 300 eV
Field of view (FWHM)	< 60 arcmin (for a collimated inst.)
Pixel size	< 500 µm × 500 µm (for a focused inst.)
Time resolution	< 10 µs
Dead time	< 0.5% (@ 1 Crab*)
Maximum source flux (steady, peak)	>300 mCrab, >15 Crab

* the Crab Nebula is the "standard candle" in X-ray astrophysics. In the 2-30 keV energy band 1 Crab corresponds to 4.4 ph · cm^2 · s^{-1}

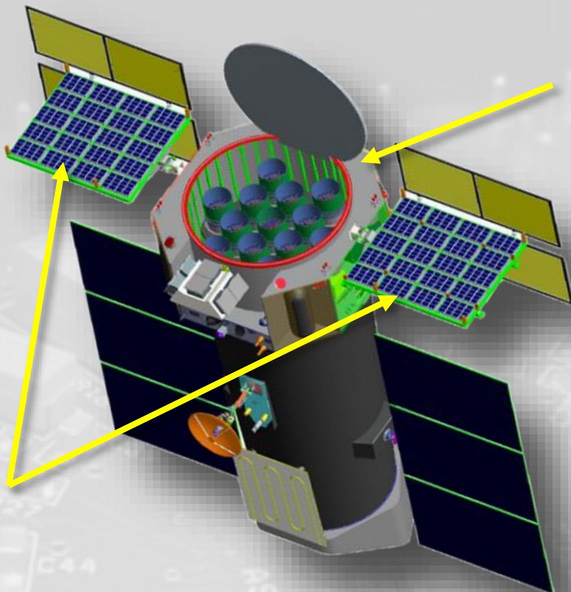

Focused instrument
large optics area
small bkg
thousands of counts/cm/s
optimal for faint sources

Collimated instrument
very large detector area
large bkg
tens of counts/cm/s
optimal for strong sources

Parameter	Requirement
Energy range	2–30 keV
Effective area	~10^4 cm^2
Energy resolution (FWHM, @ 6 keV)	< 300 eV
Field of view (FWHM)	< 60 arcmin (for a collimated inst.)
Pixel size	< 500 µm × 500 µm (for a focused inst.)
Time resolution	< 10 µs
Dead time	< 0.5% (@ 1 Crab*)
Maximum source flux (steady, peak)	>300 mCrab, >15 Crab

* the Crab Nebula is the "standard candle" in X-ray astrophysics. In the 2-30 keV energy band 1 Crab corresponds to 4.4 ph · cm^2 · s^{-1}

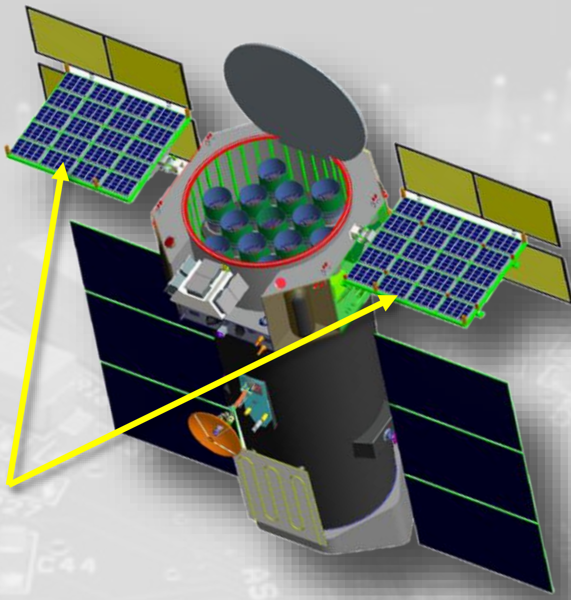

Collimated instrument
very large detector area
large bkg
tens of counts/cm/s
optimal for strong sources

- Eff. area: 3.4 m^2 @ 8 keV
- Energy band: 2-30 keV
- E res: <240 eV FWHM @ 6 keV
- Based on the LOFT/LAD design
- 40 Modules on deployable panels
- MCP collimator
- large-area SDD detector.
- Single photon, <10μs

6× RXTE/PCA,

35× XMM (coll) + hard-X response

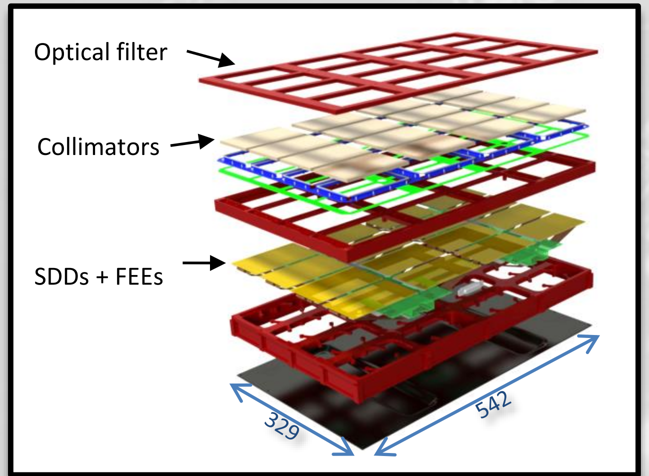

MCP coll.

SDD detector

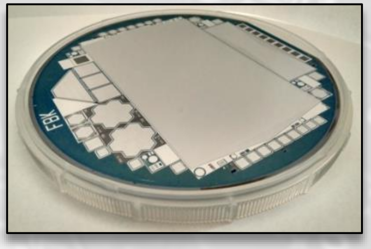

FEE PCB

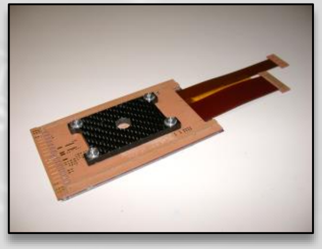

Low profile instrument, with low aeral density
(7 kg per module of 16 detectors)

SILICON DRIFT DETECTORS

ALICE ITS

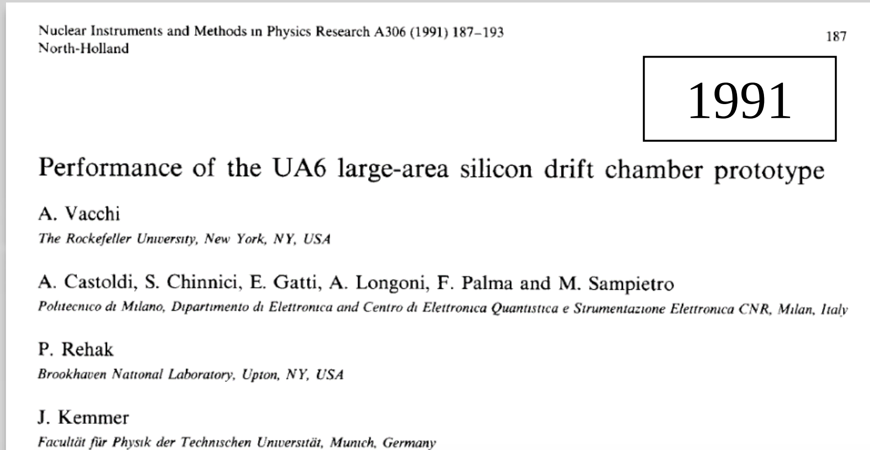

Nuclear Instruments and Methods in Physics Research A306 (1991) 187–193
North-Holland

187

1991

Performance of the UA6 large-area silicon drift chamber prototype

A. Vacchi
The Rockefeller University, New York, NY, USA

A. Castoldi, S. Chinnici, E. Gatti, A. Longoni, F. Palma and M. Sampietro
Politecnico di Milano, Dipartimento di Elettronica and Centro di Elettronica Quantistica e Strumentazione Elettronica CNR, Milan, Italy

P. Rehak
Brookhaven National Laboratory, Upton, NY, USA

J. Kemmer
Facultät für Physik der Technischen Universität, Munich, Germany

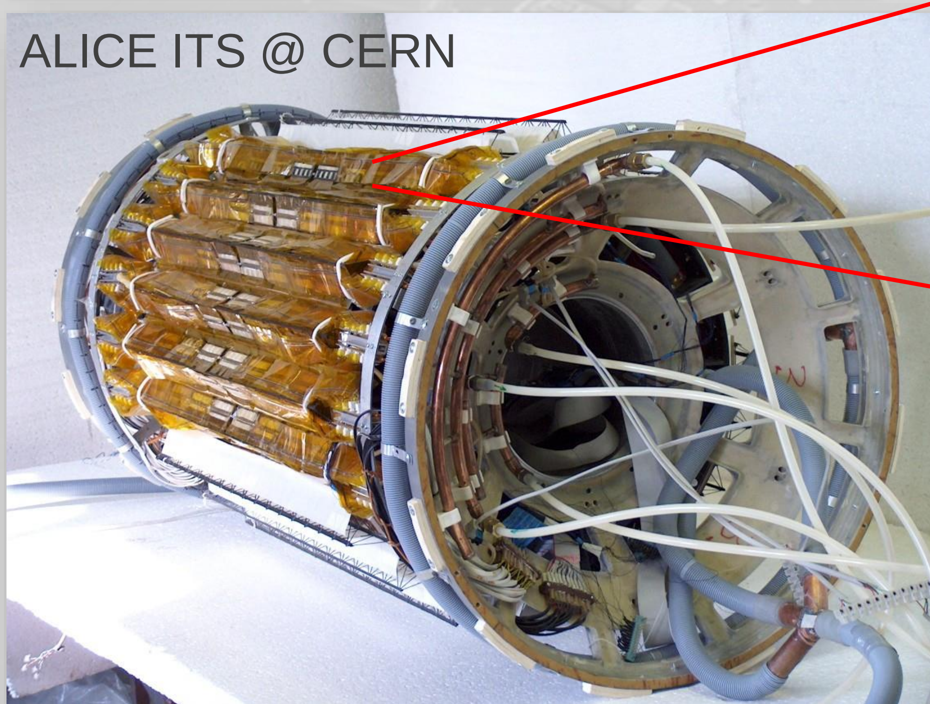

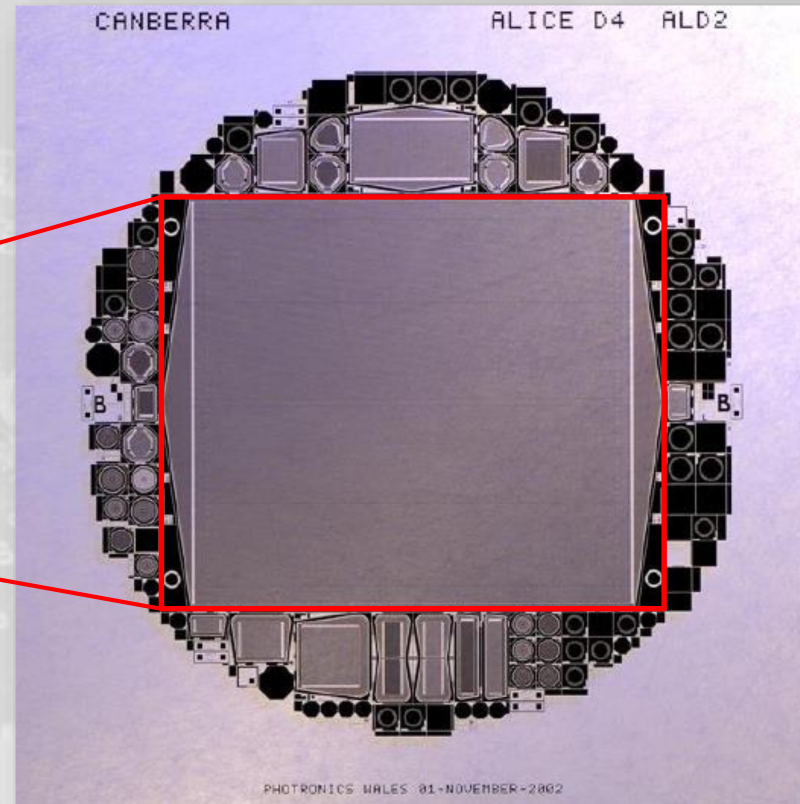

- designed to provide unambiguous 2D tracking of ionizing particles with very good resolution in a high-multiplicity environment with a very limited number of channels
- linearly scaling potentials are applied to drift cathodes to generate a constant electric field parallel to the detector surface directed outwards an array of anodes

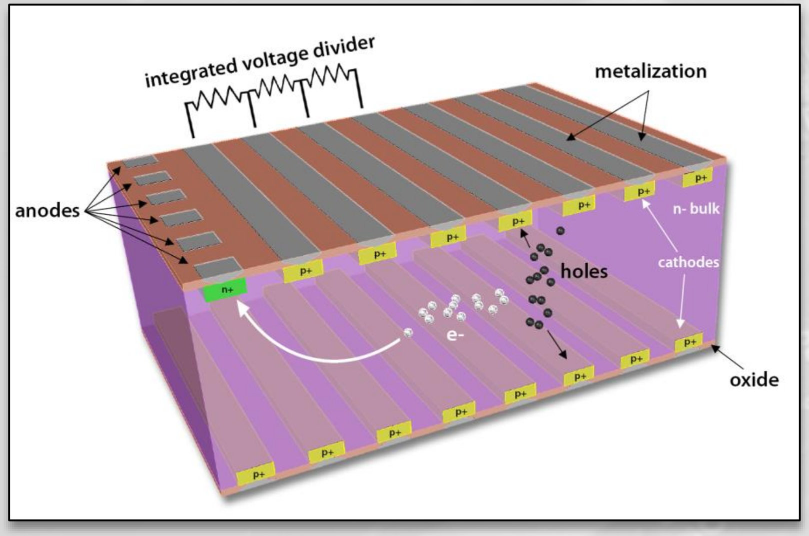

- the first coordinate is determined by the center of gravity of the signal at the anodes
- the second coordinate (drift axis) is determined measuring the time required by the electron cloud to reach the anodes

- for high position resolution the electric field must be very uniform → Neutron Transmutation Doped substrates

Large Area Silicon Drift Detectors for X-ray spectroscopy, timing and imaging designed by INFN Trieste and developed in collaboration with INAF (IAPS Rome, OAS Bo), Fondazione Bruno Kessler, PoliMi, University of Pavia, University of Bologna

More than 10 years R&D

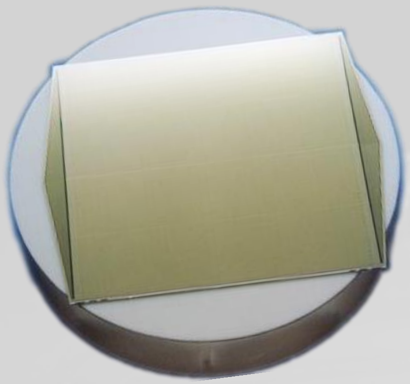

Designed by	INFN Trieste
Produced by	Canberra Semiconductor, Belgium
Geometric area	87.6 x 72.5 mm^2 (cut out from 5" NTD Si wafer)
Active area	53 cm^2
Resistivity	4 kΩ cm
Thickness	300 µm
C_{anode}	100 fF
I_{leak}	<< 1 nA/cm^2 (T_{room})

>600 detectors produced/tested (260 on ALICE ITS)

Drift Region
292 p$^+$ drift cathodes (120 µm pitch) per half
50 µm Si-SiO$_2$ gap
Al strip 15 µm wider than cathode implant

Collection
256 n$^+$ anodes (294 µm pitch)
p$^+$ pull-up cathodes on "p" side

Guard region
143 p$^+$ guard cathodes on each side

Voltage divider
8 vdiv (redundancy) p$^-$ implanted resistors
6 MΩ, 18.2 mW/cm^2 of sensitive area

MOS INJECTORS
3 arrays of MOS injectors (1 every 8 anodes)

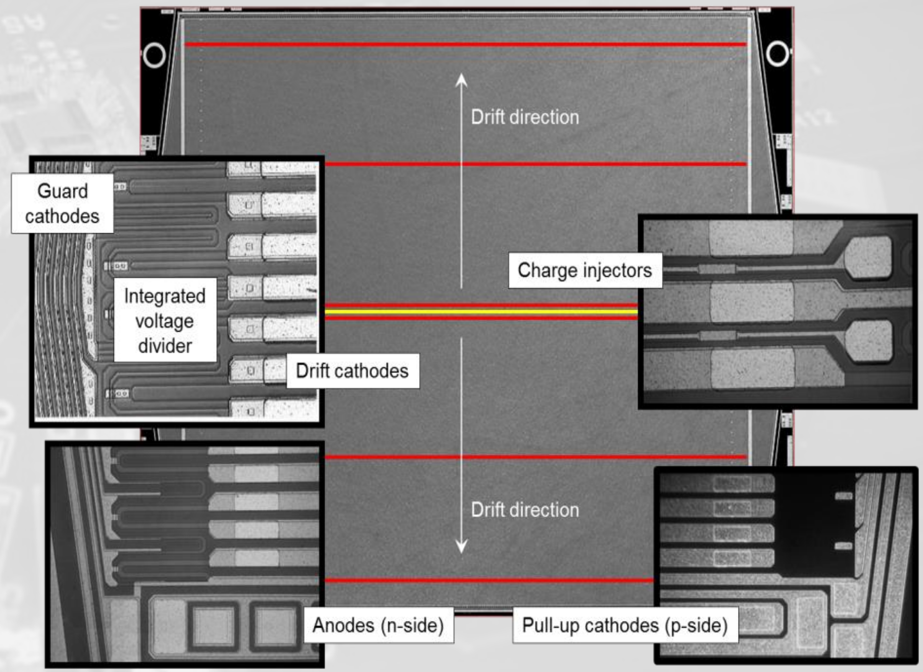

Detector development activity performed in the framework of the XDXL, ReDSoX and ReDSoX2 R&D INFN programs

Prototypes designed, manufactured and tested in collaboration between INFN, INAF and FBK.

(Rachevski et al., JINST, 2015)

Substrate optimization for x-ray detection

MATERIAL: NTD → FZ <100>
GEOMETRICA AREA (filling factor): 5″ → 6″ wafer <100>
RESISTIVITY: 4 kΩ cm→ 7-8 kΩ cm
THICKNESS (QE): 300 μm → 450 μm

Design optimization for x-ray detection and space app.

VOTLAGE DIVIDER: reduced power (18.2 → 0.5 mW/cm^2)
SURFACE CURRENT: minimization
Si-SiO_2 INTERFACE GAP: minimization
FIELD PLATE: optimization for minimal surface current
QUANTUM EFFICIENCY: optimization for low E_{ph}
ANODE PITCH: opt. for spectral-timing & imaging

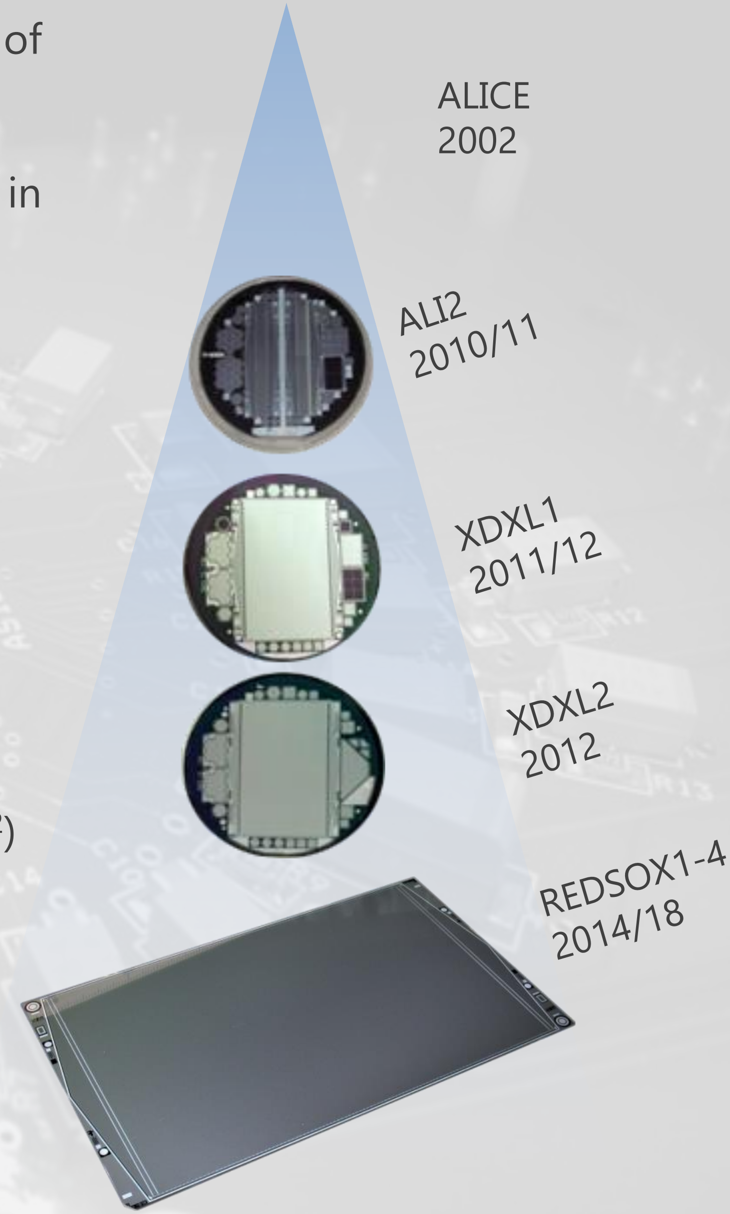

LAD SDD
LARGE AREA SDD

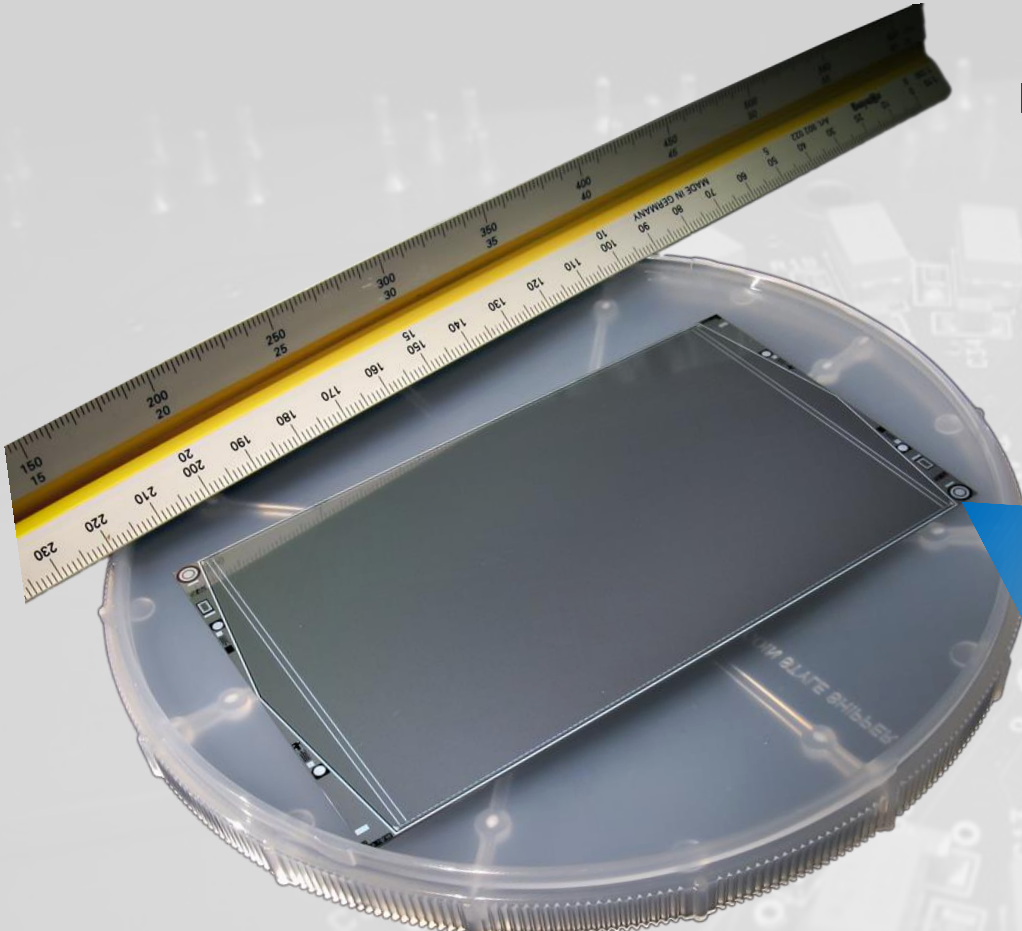

Largest monolithic SDD ever built

- First full-scale prototypes produced 2014
- Cut out from 6″ wafer
- Geometric area: 120.3 x 72.5 mm^2
- Sensitive area: **108.5 X 70.0 mm^2**
- Leakage current: **<200 pA/cm^2 @ T$_{room}$**

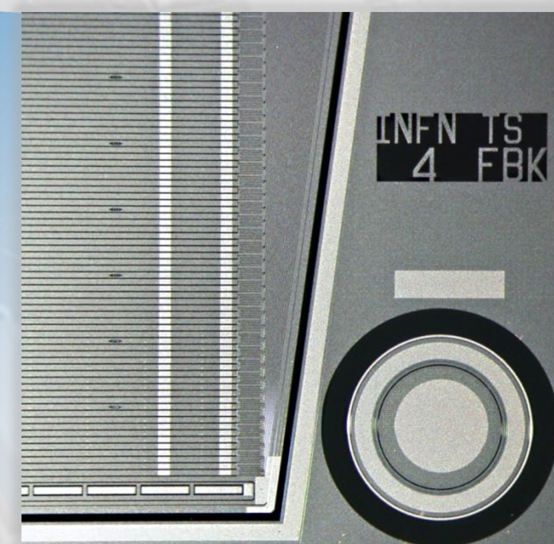

INTEGRATED SET-UP

- VEGA low-power (<500 μW/ch) ASIC designed by PoliMi & Pavia University
- PCB - designed and realized by the University of Geneva (DPNC)
- NI TE - INAF/IASF Bo, University of Bologna
- XDXL2, ReDSoX1 and ReDSoX 3 detectors

(Ahangarianabhari, 2014; Campana, 2014, Ambrosino in prep)

Spectroscopic performance characterized in IAPS Rome X-ray facility

I_{leak} ~ 5pA/anode (~LOFT/LAD EoL)
single anode events selected

^{55}Fe with CMN correction (**205 eV FWHM**)
18.1 e^- rms taking into account residual CMN

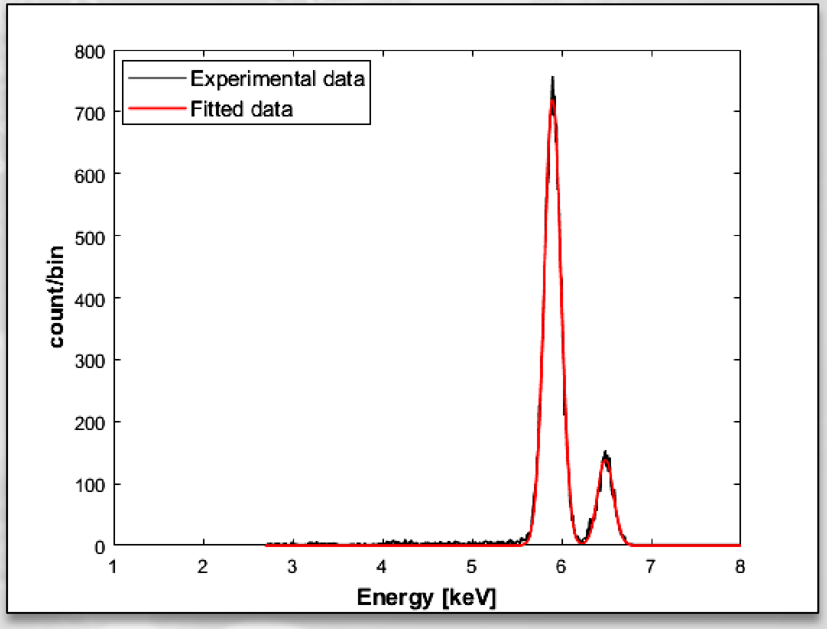

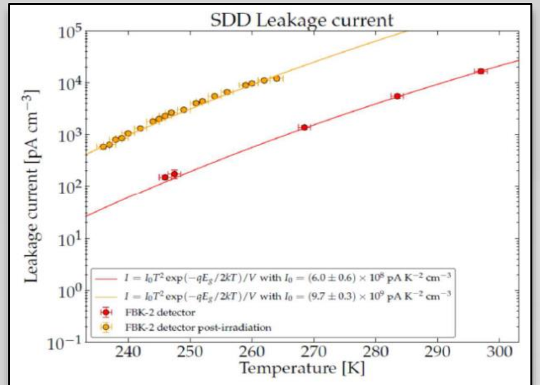

Irradiated @ PIF (PSI) with 2.5×10^9 p/cm^2 - 11.2 MeV → **120 year in 600 km/5° orbit**

At 20 °C, the measured average **increase of leakage current is 9.2 nA/anode**, the predicted increment is 8.7 nA/anode (Segneri et al. 2009), agreement within 6% .

The **TID** (1.4 krad(SiO_2)) is representative of eXTP and gives a **negligible current increase**.

Del Monte et al., 2014

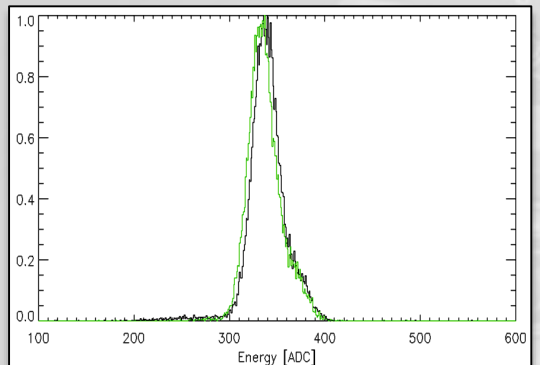

Irradiated @ PIF (PSI) with 8.9×10^8 p/cm^2 → **42 year in 600 km/5° orbit**

After irradiation **1-CCE** of **(0.65 ± 0.15)%**, expected: **0.8 %.**

Del Monte et al., 2015

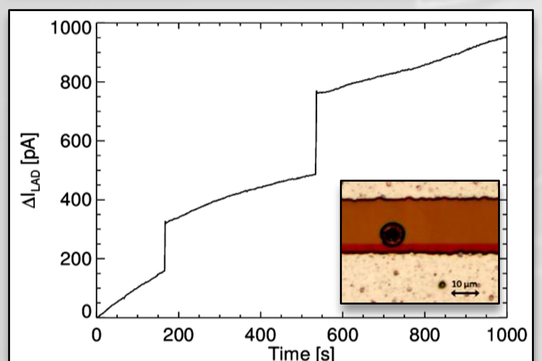

LAD expected rate: **9 x 10^{-4} impacts/yrs per SDD tile**
WFM expected rate: **2.5 x10^{-3} impacts/yrs per SDD tile**

Impact of hypervelocity particles measured at the **Cosmic Dust Accelerator Facility** of the Max-Planck Institut für Kernphysik (MPIK) in Heidelberg

Zampa N. et al., 2014

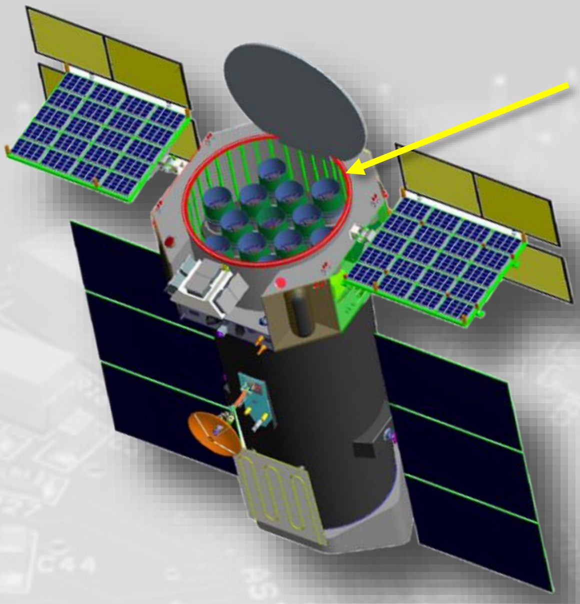

Focused instrument
large optics area
small bkg
thousands of counts/cm/s
optimal for faint sources

Parameter	Requirement
Energy range	2–30 keV
Effective area	~10^4 cm^2
Energy resolution (FWHM, @ 6 keV)	< 300 eV
Field of view (FWHM)	< 60 arcmin (for a collimated inst.)
Pixel size	< 500 μm × 500 μm (for a focused inst.)
Time resolution	< 10 μs
Dead time	< 0.5% (@ 1 Crab*)
Maximum source flux (steady, peak)	>300 mCrab, >15 Crab

PixDD

"A Fast Multi-Pixel, Integrated Silicon Detector-Read-out System for Focal Plane High Resolution X-ray Timing and Spectroscopy"

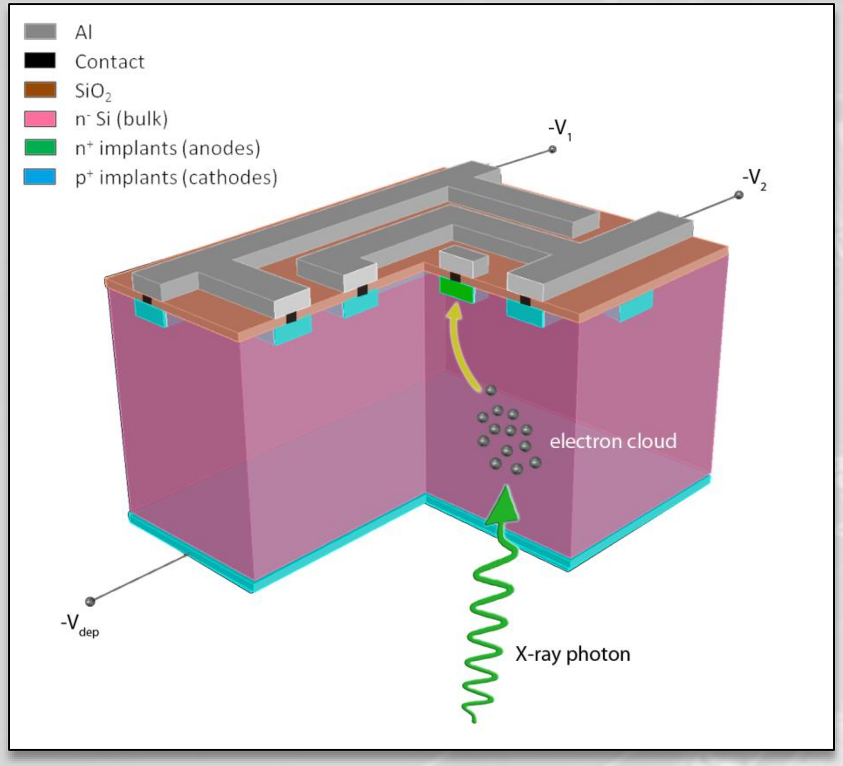

- Pixelated detector based on Si planar technology
- 500µm × 500µm pitch, 4×4 channels (1st prototype)
- 300µm × 300µm pitch, 16×8 channels (2nd prototype)
- 450 µm thick Silicon Wafer, high-resistivity (FZ <100>)
- Thin entrance window (back-illumination)
- 0.5 - 20 keV energy band
- <150 eV FWHM (@ 5.9 keV) energy resolution
- Operation at room-temperature
- Photon-by-photon (sparse) readout
- Bump-bonding interconnection for 2nd prototype

Detector design and manufacturing by INFN-Ts and FBK.
Development in collaboration between INAF, PoliMi, UniPV, KIT
Funded with contribution from INFN (under the RedSoX2 project and FBK-INFN agreement 2015-03-06), INAF (under grant TECNO-INAF-2014) and ASI (under INAF-ASI agreement 2016-18-H.0)

PIXDD DETECTOR

1° PROTOTYPE CHARACTERIZATION

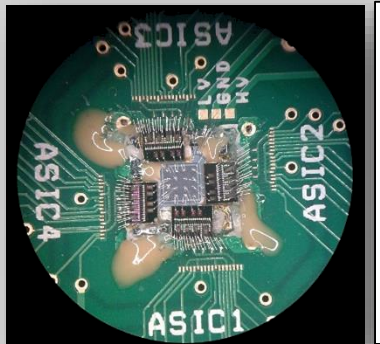

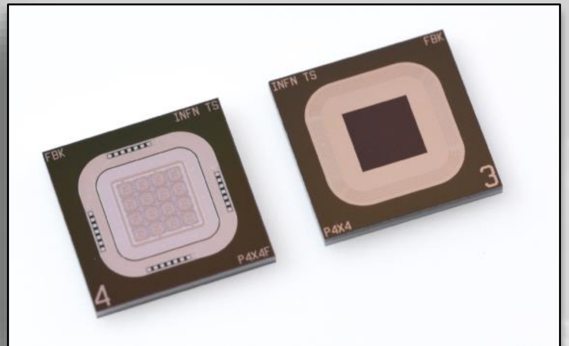

1° prototype characterized at T_{room} with an ultra low-noise CMOS charge sensitive preamplifier developed by PoliMi (Bertuccio+ IEEE 2016)

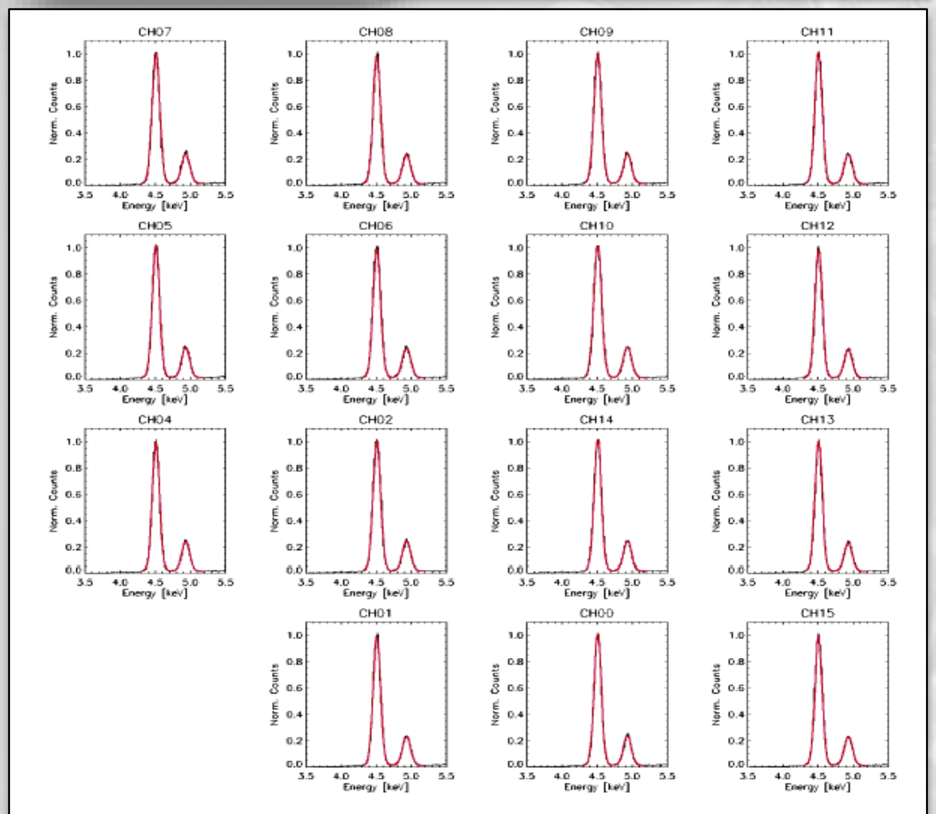

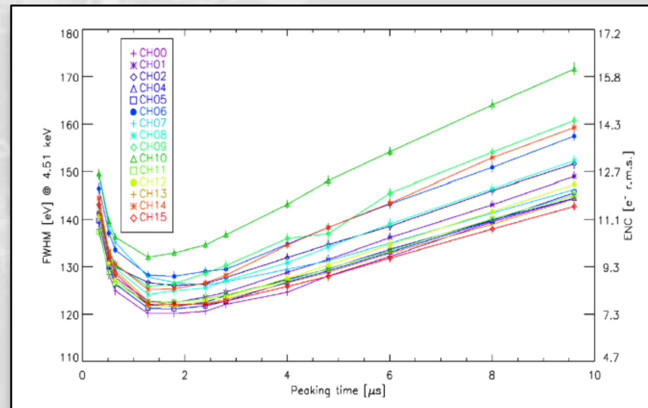

- Leakage current < 2pA/channel at +20° C
- Energy resolution at +28° C better than 150 eV FWHM @ 5.9 keV (<128 eV @ 4.5 keV)
- Optimal peaking time of 1.8 μs
- Limited charge sharing (<16%)

(Evangelista+ JINST 2018)

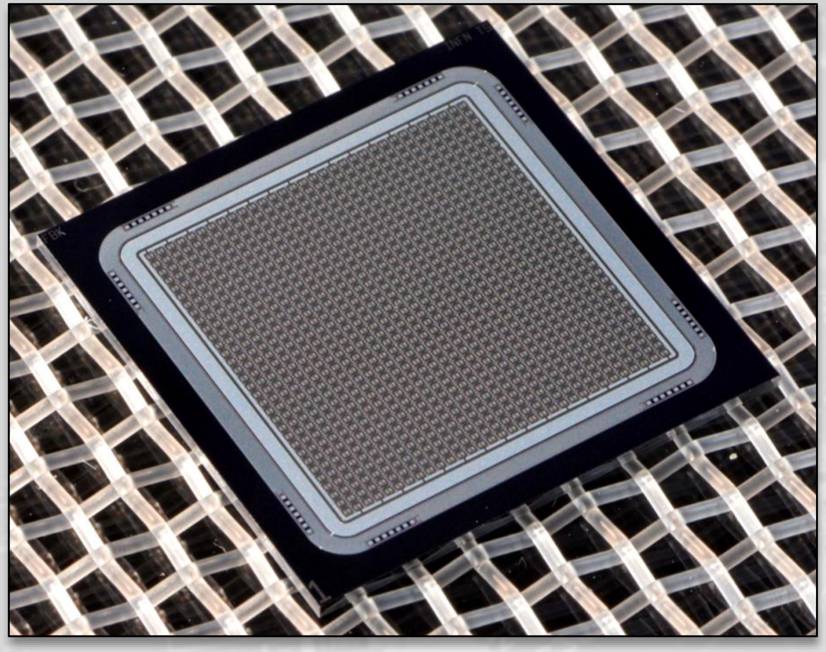

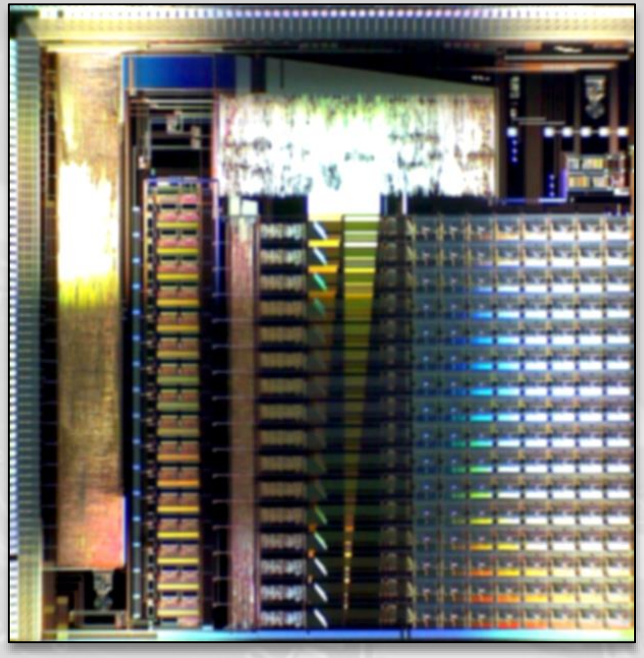

- 2nd prototype already produced and tested in probe station (INFN-Ts, FBK, TIFPA)
- 2D ASIC - RIGEL - designed by PoliMi and UniPV and produced in AMS 0.35 technology. Currently under test
- Interconnection technique developed by KIT already optimized in collaboration with INFN-Ts, TIFPA

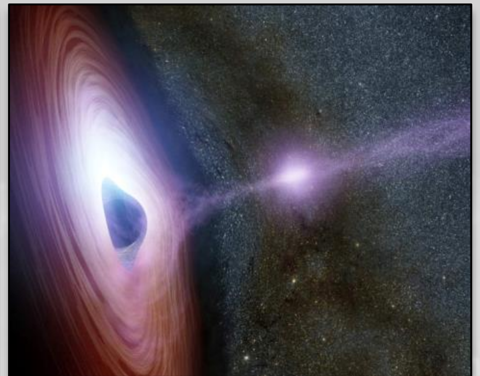

Strong field gravity

- high sensitivity
- good spectral resolution
- good timing resolution
- soft X-ray energy band
- negligible dead-time and pile-up

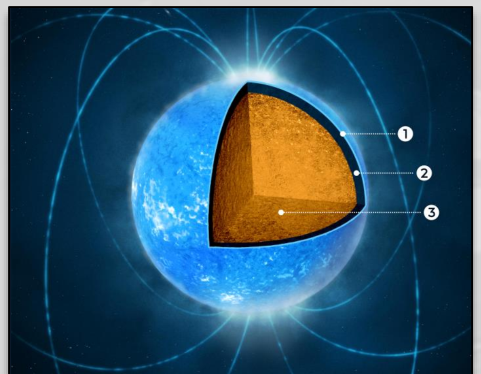

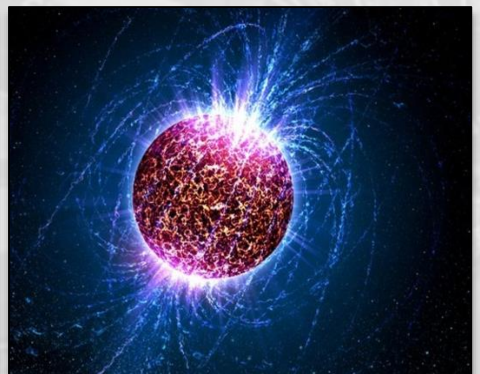

Dense matter

- high sensitivity
- average spectral resolution
- good time accuracy
- soft X-ray energy band
- negligible dead-time and pile-up

Strong magnetic fields

- high sensitivity
- soft X-ray polarimetry

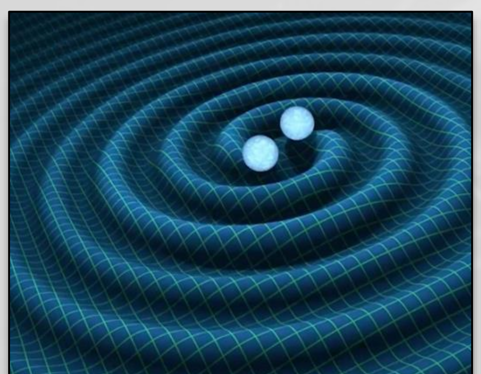

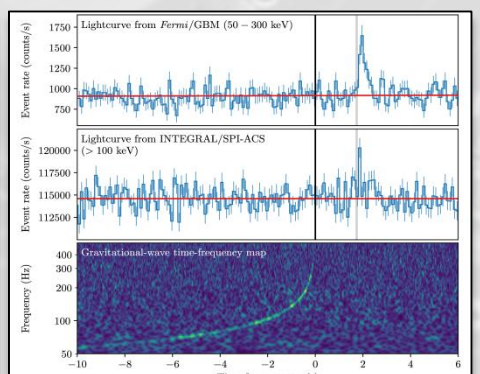

GW and multi-messenger astronomy

- large field-of-view
- good sensitivity
- good angular resolution (PSLA)
- soft/hard X-ray energy band

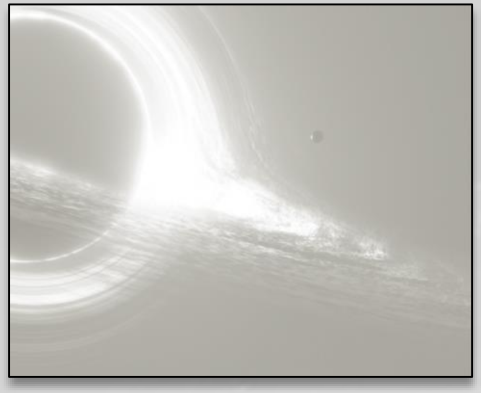

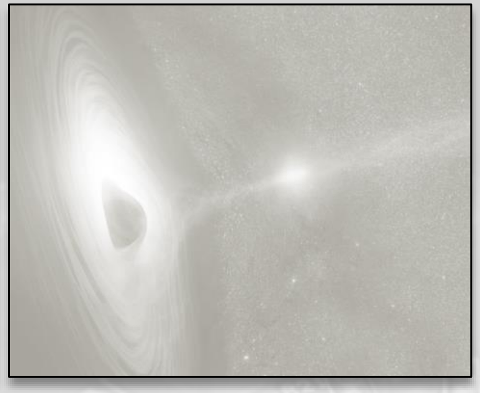

Strong field gravity

- high sensitivity
- good spectral resolution
- good timing resolution
- soft X-ray energy band
- negligible dead-time and pile-up

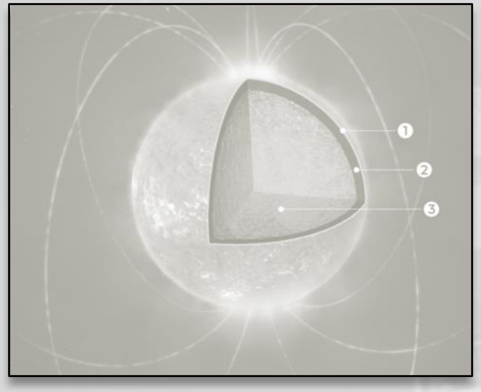

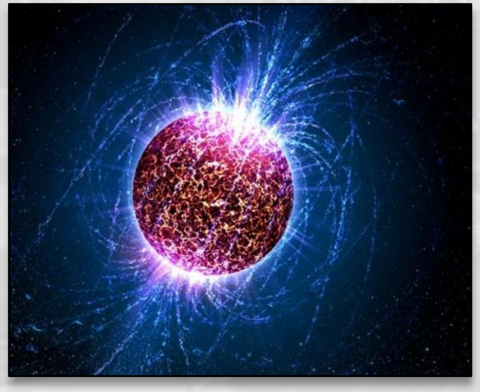

Dense matter

- high sensitivity
- average spectral resolution
- good time accuracy
- soft X-ray energy band
- negligible dead-time and pile-up

Strong magnetic fields

- high sensitivity
- soft X-ray polarimetry

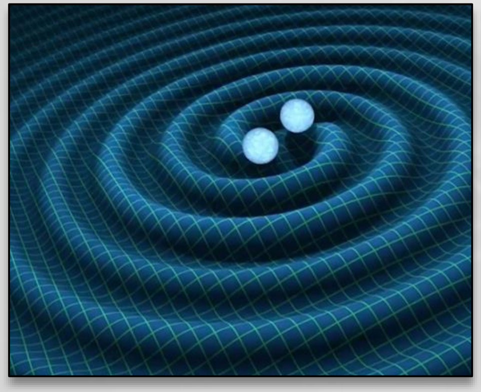

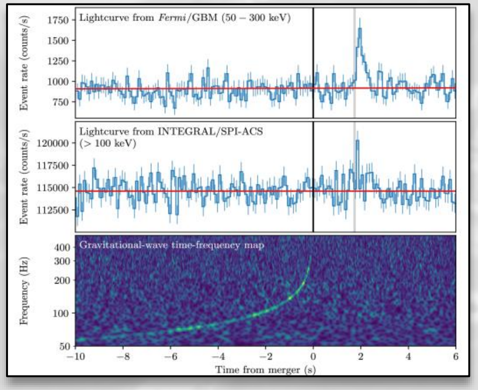

GW and multi-messenger astronomy

- large field-of-view
- good sensitivity
- good angular resolution (PSLA)
- soft/hard X-ray energy band

WIDE FIELD MONITORING

HERMES - ASI

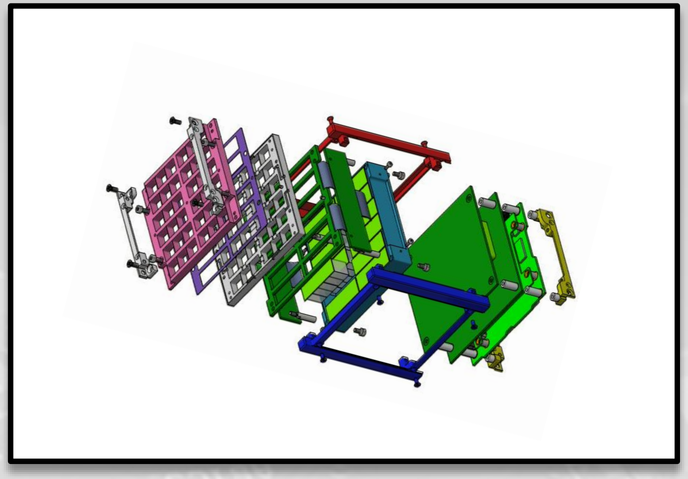

Approved – Launch mid 2020

eXTP - CAS

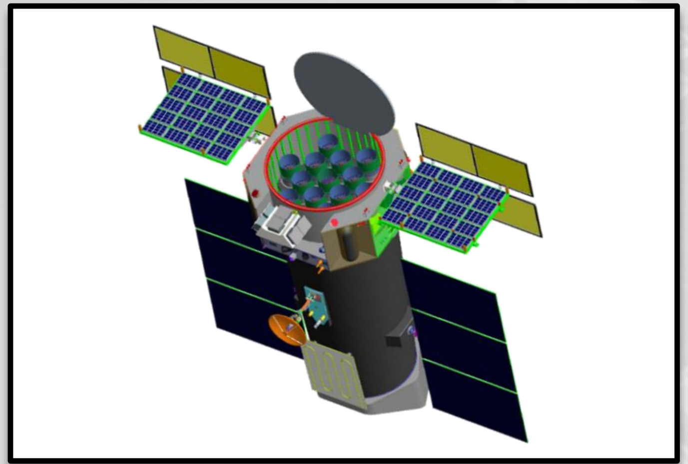

Phase B in 2019 – Launch ≥ 2025

STROBE-X - NASA

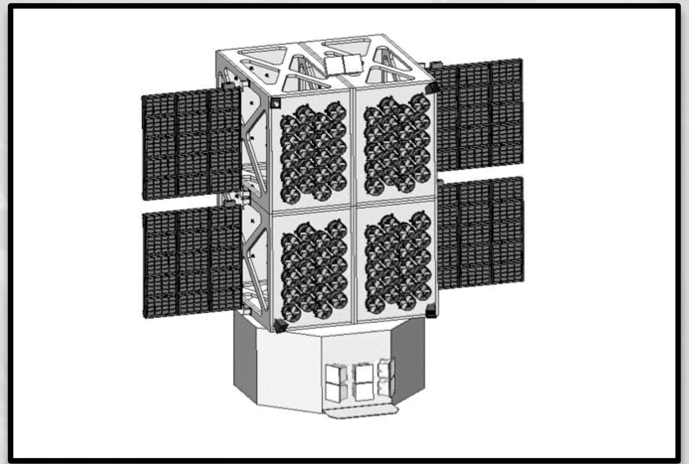

Study for Decadal 2020 survey

Compact and light-weight approach to wide field (1-2 sr FoV) imanging in X-rays. Several coded aperture instrument flown (AGILE, Swift, Integral, RXTE, Astrosat, …)

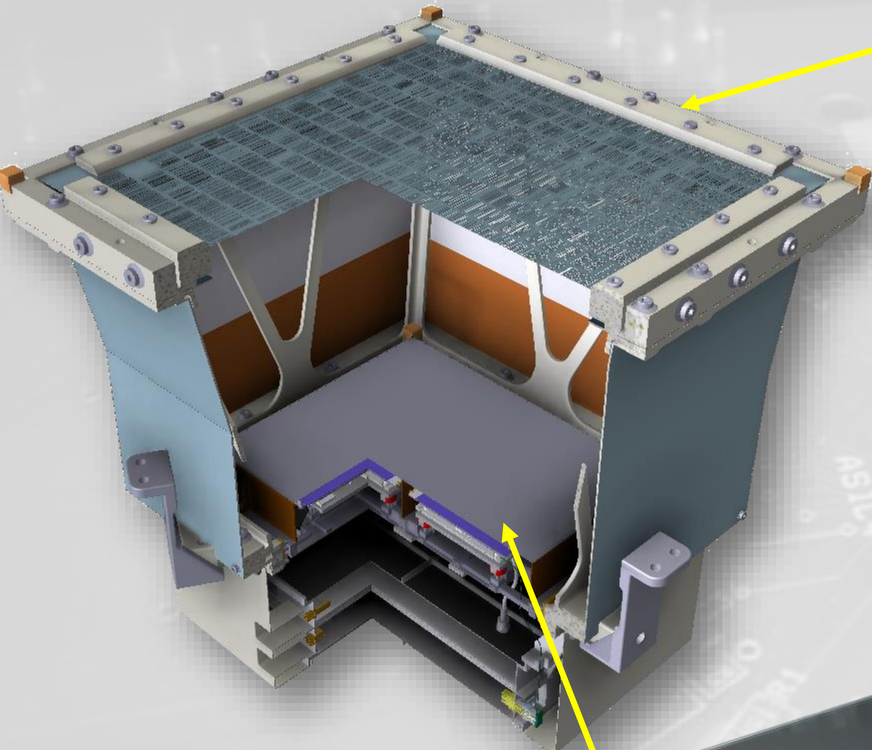

Coded mask

Concept of pin-hole camera

Apertures arranged to ensure delta-like autocorrelation function (i.e. unambiguous determination of the source position from shadowgram)

Large Area SDD

Similar design to LAD SDD, but smaller anode pitch to exploit segmentation of the (diffused) charge cloud

CODED APERTURE IMAGING

THE LARGE AREA SDD APPROACH

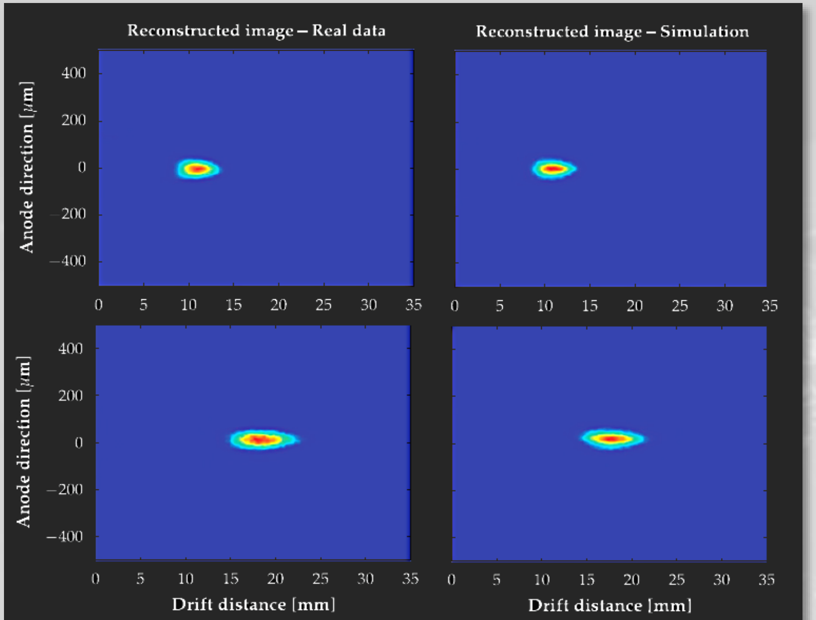

Anode segmentation provides 1D photon absorption position with high **spatial resolution (tens of μm)**

e- cloud width (**σ**) encodes information on **drift distance** → 2D (asymmetric) spatial resolution

$$\sigma = \sqrt{2Dt+\sigma_0^2} = \sqrt{2\frac{k_B T}{qE}x+\sigma_0^2}$$

- D → diffusion coeff.
- t → drift time
- k_B → Boltzmann c.
- q → electron charge
- x → drift length
- E → Efield strength

Campana et al., 2011

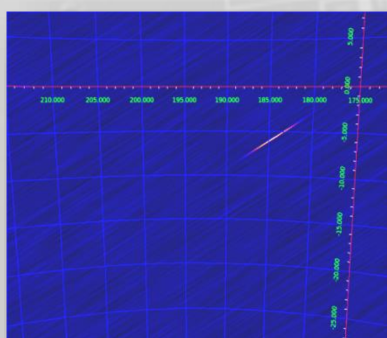

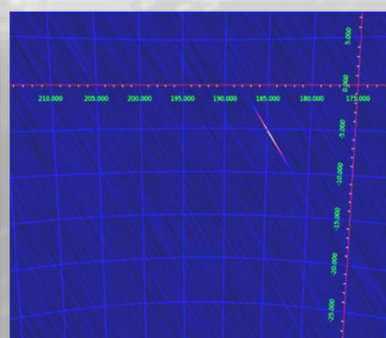

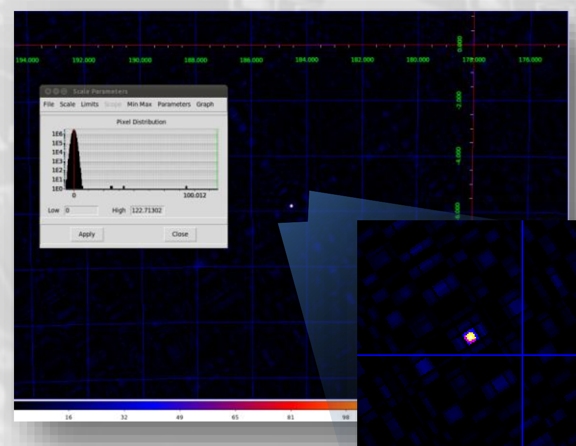

TRIANGULATION

Triangulation is an old concept in X-ray and γ-ray astronomy

- GRBs discovered by VELA satellites (launched in 1963 to monitor Partial Test Ban Treaty)
- IPN (Inter Planetary Network) working efficiently since 1976 to position GRBs

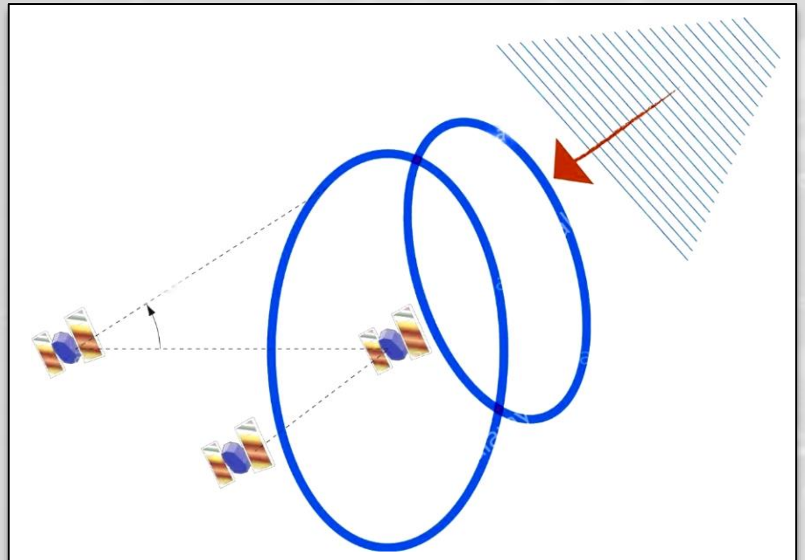

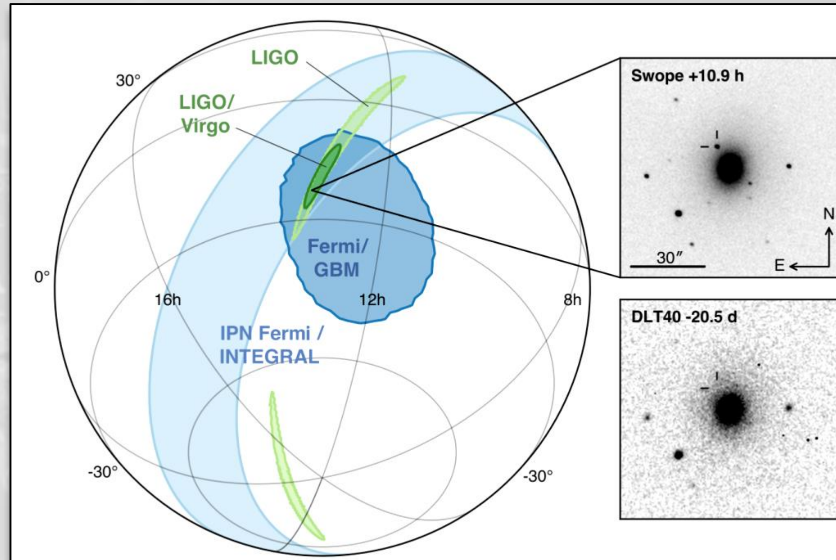

The principle is to measure GRB positions through delays between photons arrival times (light curve cross-correlation):

$$\sigma_{\rm pos} = \sigma_{\rm ccf}\,\frac{c}{B\sqrt{N-1-2}}$$

If we consider 4 satellites (N=4), an average baseline B=7000 km and a σ_{CCF} of 500 us the expected position error is ~1°. With larger constellations (N=50/100) it is possible to obtain arcmin-level position accuracy.


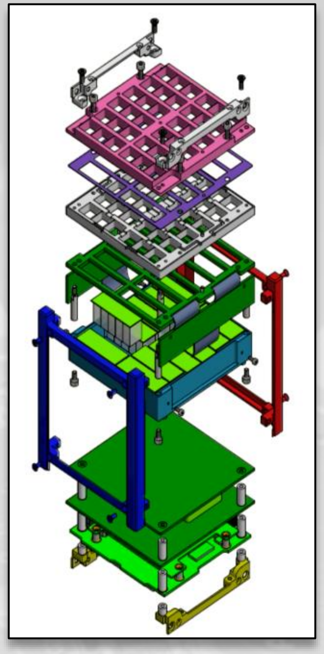
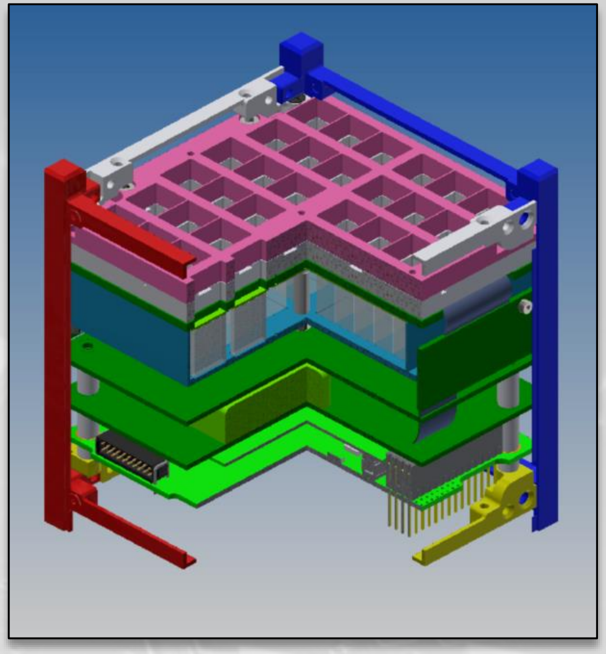

HERMES is a constellation of 3U CubeSat satellites (spacecraft 10×10×30 cm^3), each one equipped with a two-stage segmented detector (1U for P/L):

- 120× rectangular SDD (6×7 mm^2 cells) front illuminated (X-rays). Energy band: 3-20 keV
- 60× GAGG scintillators crystals (12×7×15 mm^3) for γ-ray conversion. Scintillator light is read-out by the same SDD (back illumination). Energy band: 20 keV -2 MeV

Plus a local miniaturized atomic clock to provide high accuracy photon time tagging

First set of 6 (3+3) satellites funded by ASI and H2020. Launch between 2020-2022

THANK YOU

SPARE SLIDES

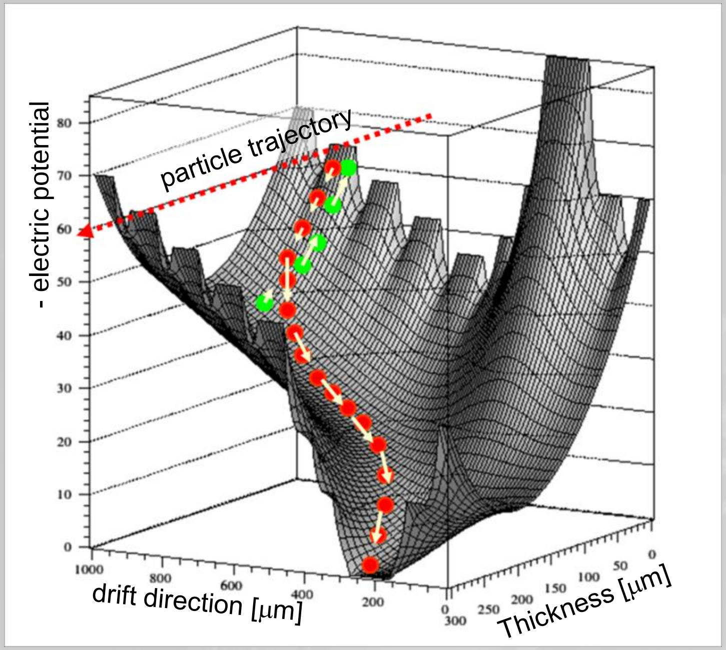

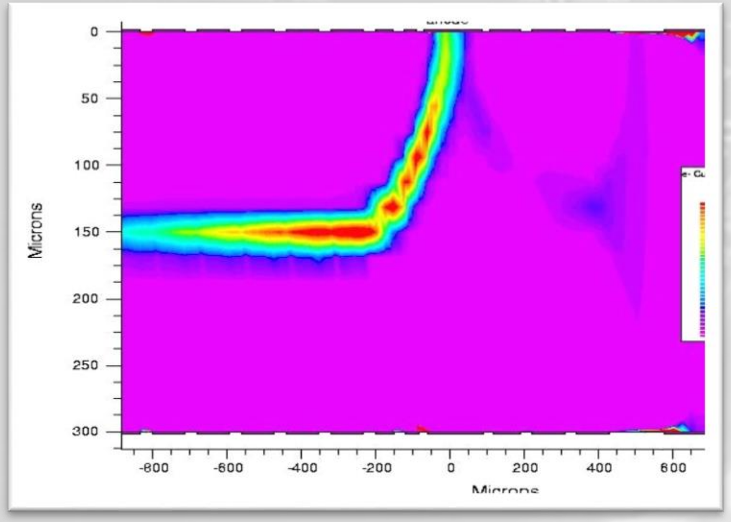

Cloud of e$^-$-h created by x-ray photon interaction (3.65 eV/e-h pair)

e$^-$ quickly focused in the middle plane of the detector (sideward depletion) and carried towards the anodes thanks to the drift field. Holes collected by cathodes

Because of diffusion, the size of the electron cloud increases with time before reaching the collecting anodes, up to several hundreds of μm

The Gaussian-shaped electron cloud propagates along the drift direction and reaches the read-out anodes with a width σ which can be expressed as:

$$\sigma = \sqrt{2Dt + \sigma_0^2} = \sqrt{2\frac{k_B T}{q}\mu\frac{x}{\mu E} + \sigma_0^2} = \sqrt{2\frac{k_B T}{qE}x + \sigma_0^2}$$

$D \rightarrow$ diffusion coeff.
$t \rightarrow$ drift time
$k_B \rightarrow$ Boltzmann c.
$q \rightarrow$ electron charge
$x \rightarrow$ drift length
$E \rightarrow$ electric field strength

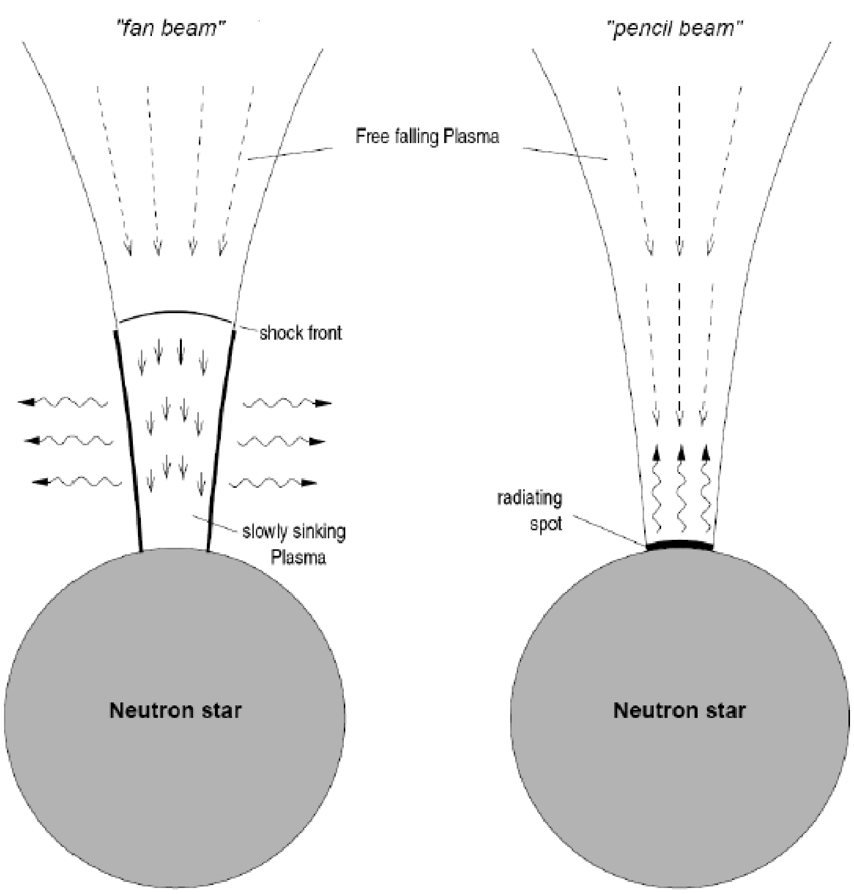

High accretion rate: *shock is formed*, plasma is decelerated to subsonic speed and heated. *The Plasma then sinks to the NS surface*. Emitted photons can only escape perpendicularly to the column forming a wide *Fan beam.*

Lower accretion rate No shock is formed, *plasma is decelerated onto the neutron star surface* by Coulomb collisions; photons are generated by Bremsstrahlung and Compton Cooling. They can escape along the accretion column, generating *a pencil beam*

ACCRETING X-RAY PULSAR

Eight values of energy, from bottom to top:

1.6, 3.8, 9.0, 18.4, 38.4, 51.7, 84.7 keV.

Pencil beam:
I–P anticorrelation

Fan beam:
I–P correlation

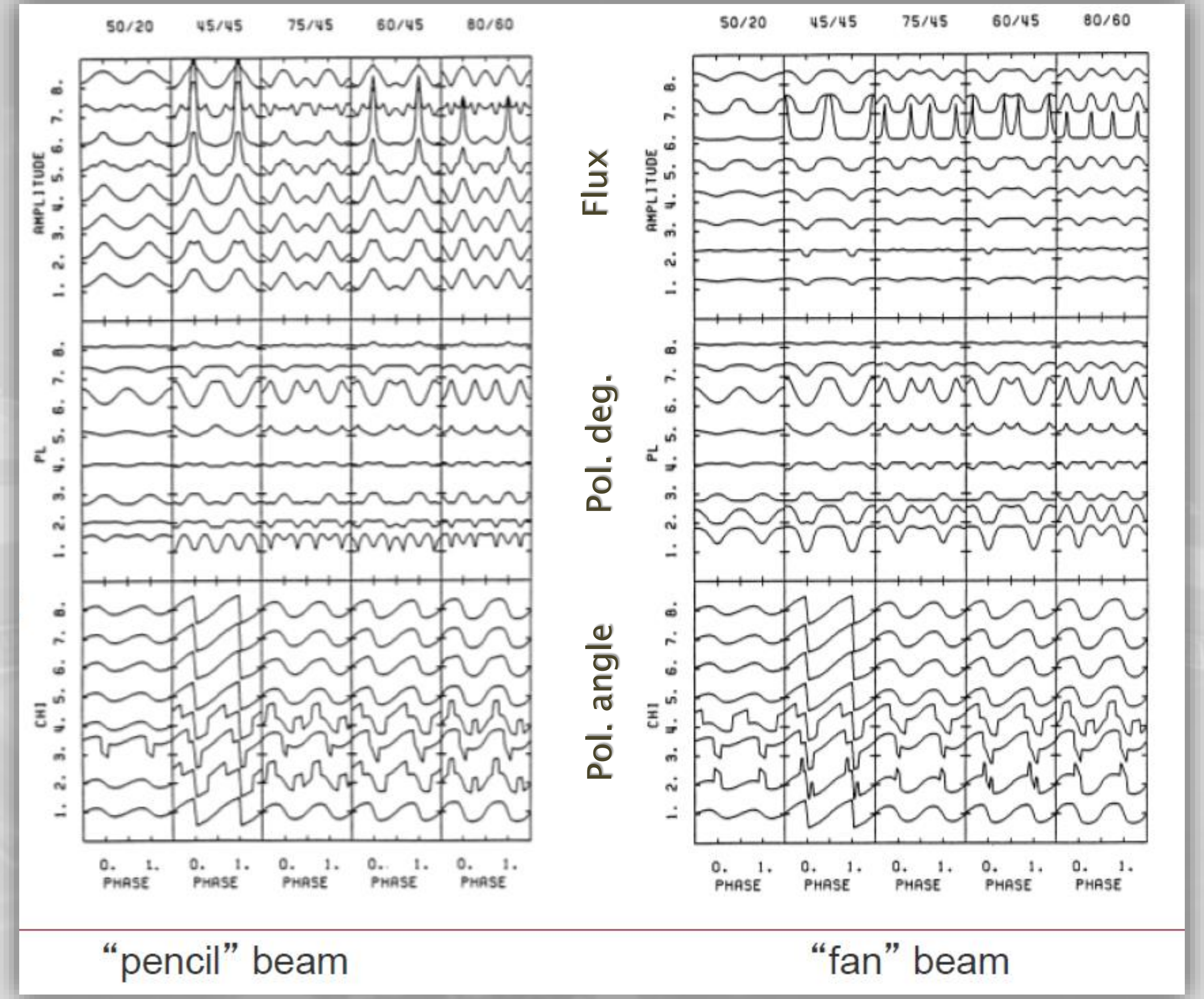

Meszaros et al. 1988

The strong force determines the state of nuclear matter from atomic nuclei to neutron stars

- a major open problem in modern physics
- progress driven by experiment and observation

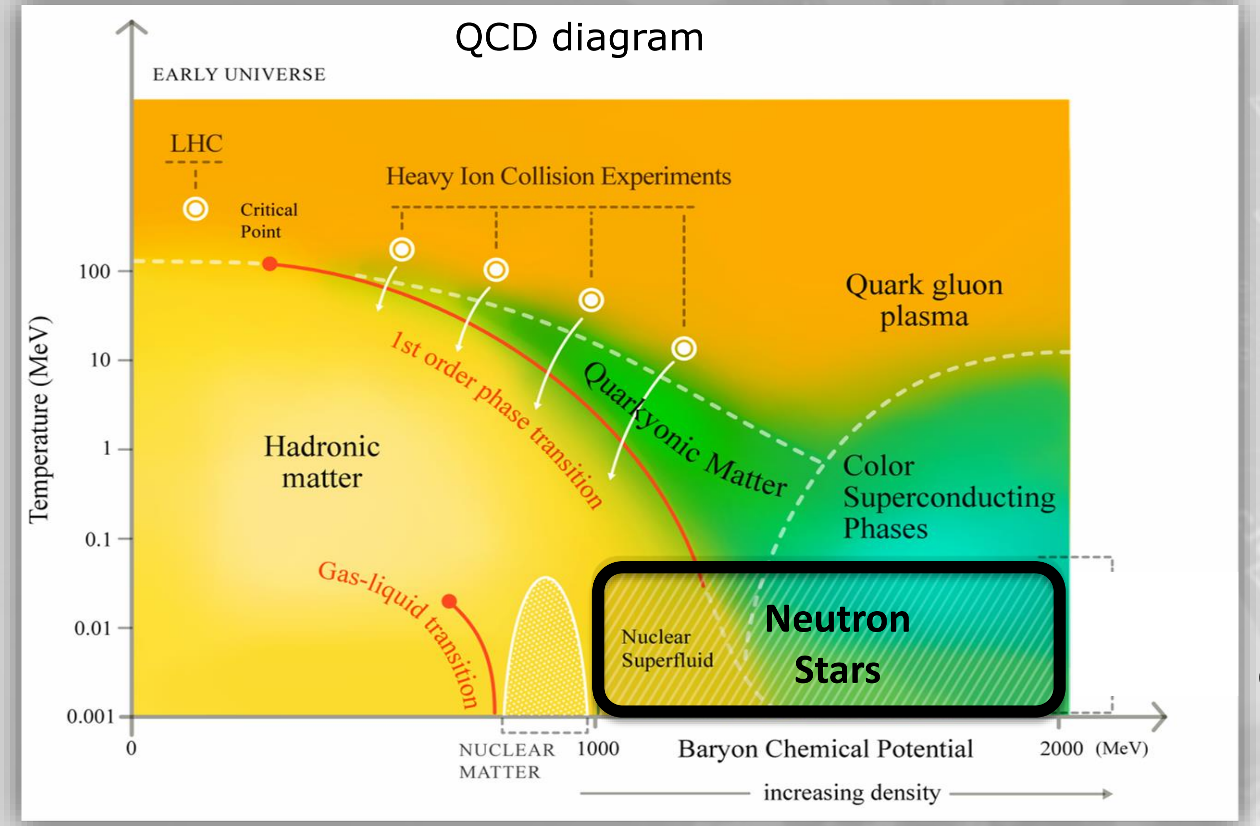

Neutron stars contain the **densest** and most **neutron-rich** matter **in the Universe**.

OSO-8

FIRST AND ONLY POLARIMETER EVER FLOWN

The first and only X-ray polarimeter ever flown was on-board OSO-8 (1975-1978) based on Bragg diffraction on Graphite crystals

- 2× parabolic crystals
- 2.4-2.8 keV & 4.8-5.6 keV
- μ=0.93
- spin period 10 s

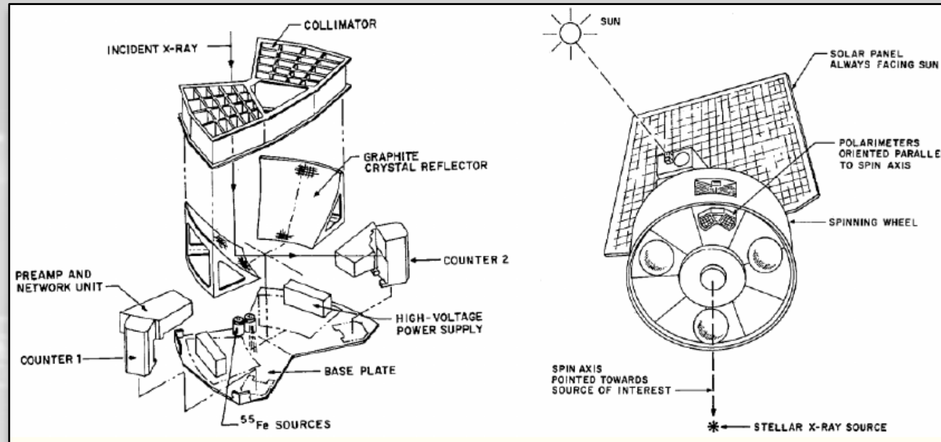

The first polarimetric measurement

- Crab Nebula
- P = 19.22 ± +/- 0.92%,
- Φ_0 = 155.79° +/- 1.37°

12 days of observation in 2 years
71.2 hours of good data, 71.3 hours of bkg
SNR of 10 at 2.6 keV, 2 at 5.2 keV

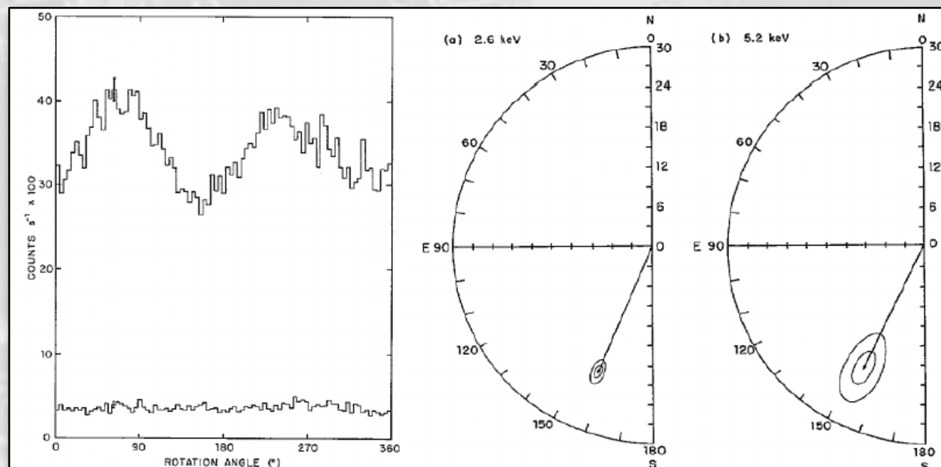

and the modulation curve was not a cosine square...

ALICE (a) and ALI2 (b) integrated voltage divider designs

a) **8 parallel voltage dividers,** large current (unaffected by hole leakage current) → **high power consumption** (not suitable for spaceborne experiments)

b) **single VD** (45 MΩ @ 20° C) → **0.5 mW/cm²** **(was 18.2 mW/cm²)**

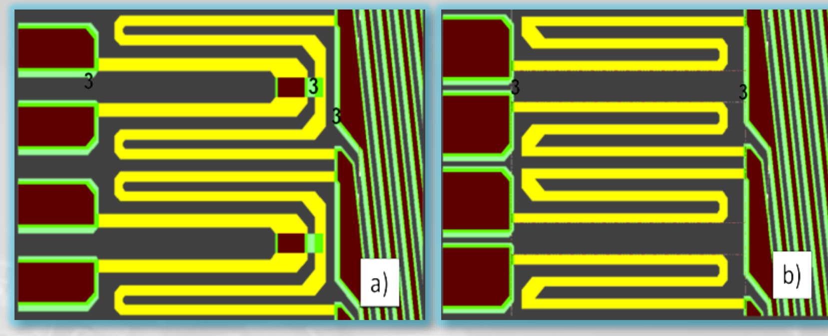

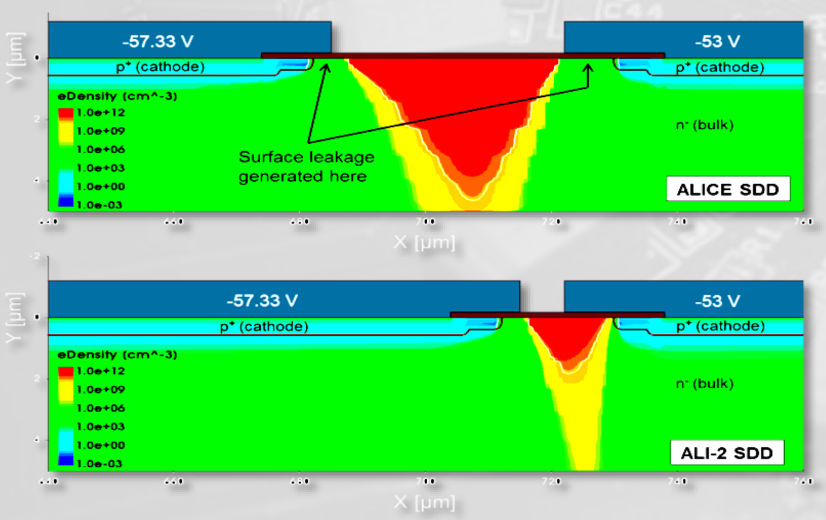

minimization of bulk generation not sufficient to reach energy resolution goals (LAD)

→ surface current as small as possible

moreover, H_2O lower Q_{ox} (~10^{11} ions/cm²)

cathode gaps reduced from 50 µm to 20 µm

I_{leak} measured in a set of test structures with different FP width.

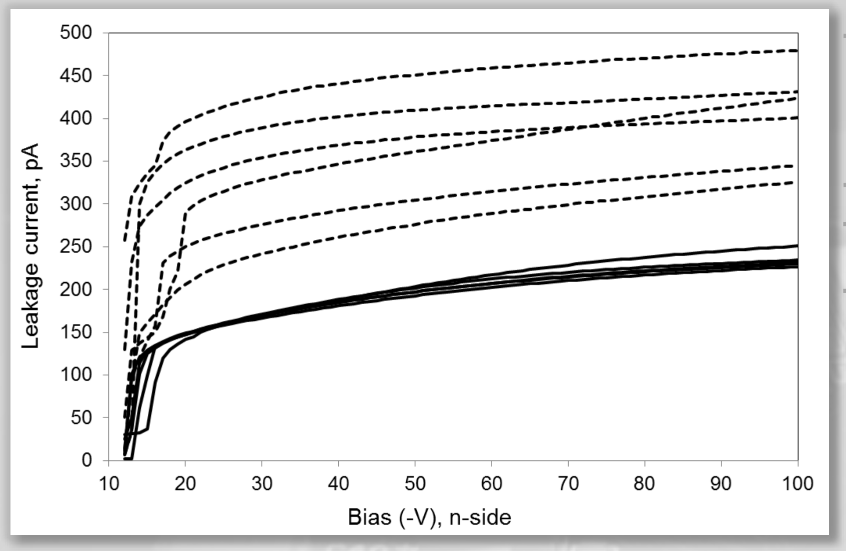

FP extending 5 µm beyond the implant edge

FP completely covering the SiO_2 gap

Positive FP covers the gap between cathodes (2nd prot.) and guards (3rd prot.) → I_{leak} stabilized, det. stability against external conditions

Detector QE optimized for low energy photons response by:

→ **gap minimization** (reduction of **low |E|** region under the gap)

→ **reduction** of the **thickness** of:
- passivation (also changed Polyamide with SiO_2)
- metal
- junction depth

QE modulation measured in the IAPS Rome X-ray facility with collimated (~100 um FWHM) monochromatic beam

LAD SDD

QUALIFICATION: NIEL, TID

XDXL2 irradiated @ PIF (PSI) with 2.5 × 10^9 p/cm^2 - 11.2 MeV (6 MeV FWHM) →**120 year in 600 km/5° orbit**

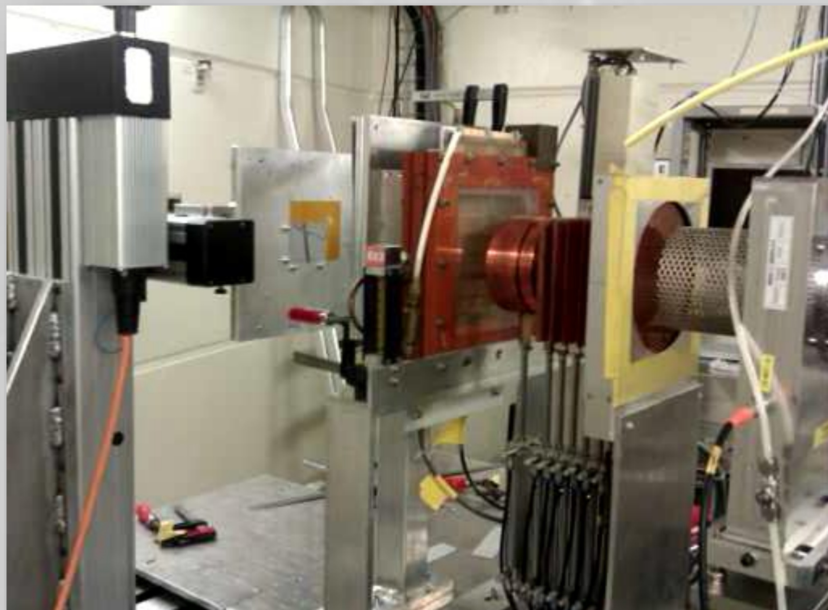

Del Monte et al., 2014

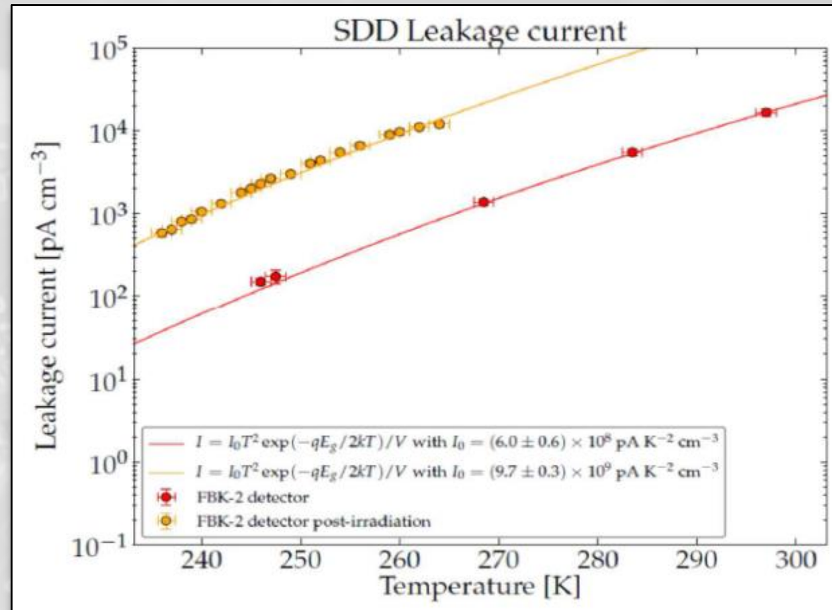

At 20 °C, the measured average increase of leakage current is **9.2 nA/anode**, the predicted increment is **8.7 nA/anode** (Segneri et al. 2009), **agreement within 6% .**

The TID (1.4 krad(SiO_2)) is representative of eXTP and gives a **negligible** current increase.

The annealing follows (2σ) the prediction (Moll et al., 2002).

LAD SDD

QUALIFICATION: CHARGE COLLECTION EFFICIENCY

$1 - CCE \sim \beta\, \varphi\, t_c$ with $\beta \sim 5.6 \times 10^{16}\ cm^2\ ns^{-1}$ @ -10° C, tc ~ 5 μs

Fluence of 8.9×10^8 p/cm² (**10 times** the **nominal fluence** received by the LAD SDDs in 4.25 years 600 km, 5° LEO)
Increase of the bulk leakage current of 6.2 nA/anode at 20 ° C (no annealing).

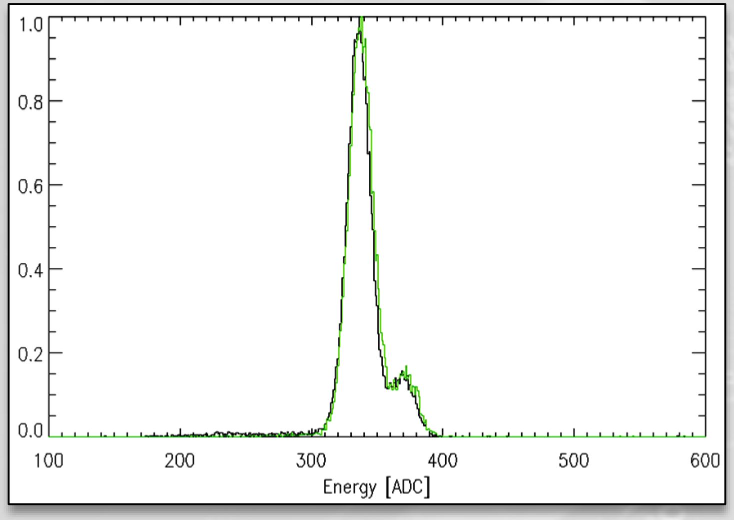

before → after

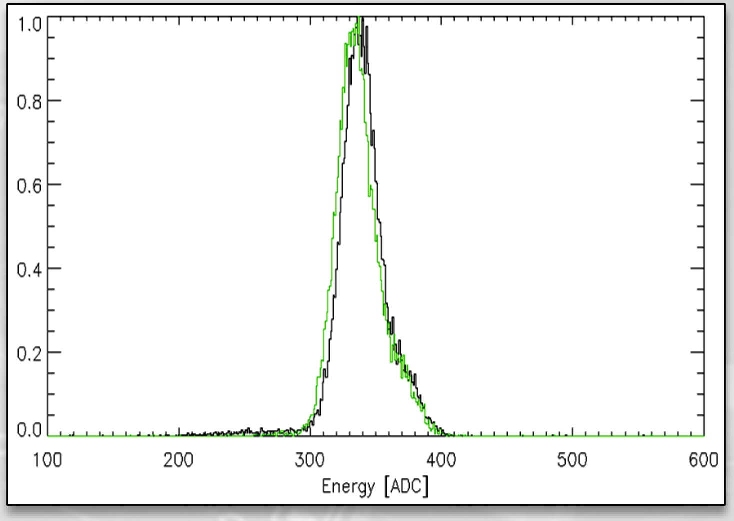

Fit of the ^{55}Fe line at 5.9 keV; Measurements at -38 °C to reduce the I_{leak} after irradiation (NIEL)

8 anodes are connected to a FEE with JFETs. charge on 3 adjacent anodes summed up to account for the charge diffusion.

After irradiation **1-CCE** of **(0.65 ± 0.15)%**, expected: **0.8 %.**

(Del Monte et al., 2015)

Impacts of micrometeroids and orbital debris (MMODs) important for orbiting experiments, especially if characterized by a large FoV (i.e. WFM)

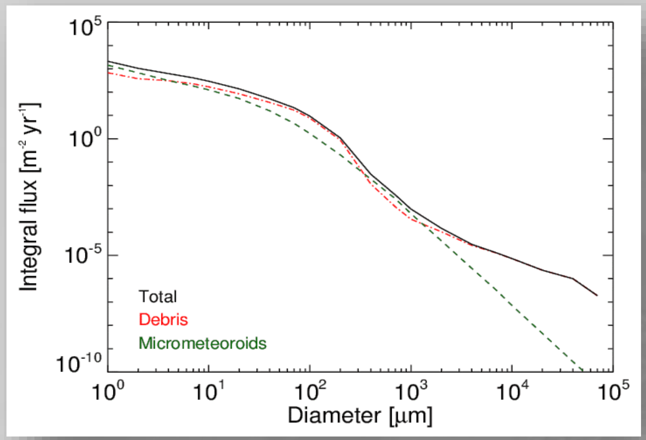

Integral flux of MMODs at the LOFT orbit.

Average values considered:

- micrometeoroids: 2.5 g/cm^3, 20 km/s
- debris: 2.8 g/cm^3, 13km/s

LAD expected rate: **9 x 10^{-4} impacts/yrs per SDD tile**
WFM expected rate: **2.5 x10^{-3} impacts/yrs per SDD tile**

Effects of the impact of hypervelocity particles measured at the **Cosmic Dust Accelerator Facility** of the Max-Planck Institut für Kernphysik (MPIK) in Heidelberg (Zampa N. et al., 2014).

Accelerator operated in "single shot", Iron grains (7.9 g cm^3) Different velocities and sizes

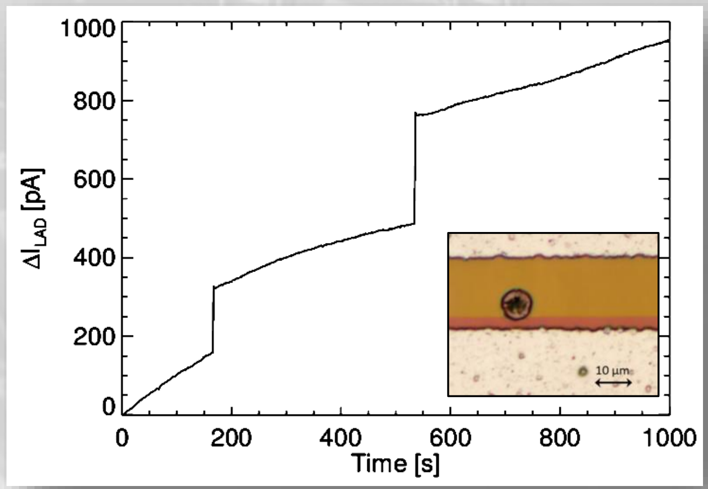

I_{leak} increase on the SDD (LAD half) with two impacts of particles with a velocity of 2 km/s and a diameter of 2 µm.
Penetration depth is 3 µm (Cour-Palais formula)